VELOCITY PROFILES AND PUMPING CAPACITIES OF TURBINE TYPE IMPELLERS

A

THESIS

BY

R. G. COOPER

Department of Chemical Engineering - McGill University

Under Supervision of Dr. D. Wolf

Submitted to the Faculty of Graduate Studies and Research of McGill University in partial fulfillment of the requirements for the degree Master of Engineering

McGill University

April, 1966

SUMMARY

Velocity profiles of propeller and turbine type impellers were measured in both air and water using a hot wire anemometer probe, and two and three dimensional pitot tubes. These pitot probes were particularly suitable for this work, since they permitted the measurement of velocity and inclination of flow in the turbine jet, from which the radial and tangential velocity components were evaluated. The velocity profiles and pumping capacities of propellers were checked, and agreed closely with the results of other researchers, thus serving as a check on the experimental technique.

A variety of geometrically similar turbines were studied with D:W:L = 20:4:5. The shape of the radial velocity profile was independent of rotational speed and independent of turbine diameter. The radial profiles were parabolic in nature, while the tangential profiles were flatter. Profiles obtained for both water and air were similar. The centreline radial velocities varied linearly with turbine speed for a given turbine.

Pumping capacities of turbines were calculated from the radial velocity profiles, and the pumping capacity was found to vary linearly with turbine speed, and almost linearly with the cube of the turbine diameter for geometrically similar turbines.

Velocity measurements were also made at different

radial locations in the turbine discharge jet. The flow becomes more radial in direction, and the radial profiles tend to a plug shape with increasing radial distance. The volumetric flow rate increases with radial distance to a limiting value of 1.8 times the periphery pumping capacity.

The effect of turbine blade width on velocity profiles and pumping capacities was investigated. Pumping capacities increase linearly with blade width, but tend to a limiting value at higher blade widths.

The pumping capacity was used to effectively correlate mixing data obtained from the work of other researchers, such as intensity of segregation, concentration fluctuations and power requirements.

Qualitative proof of the flow patterns around the impellers was obtained by using smoke as a tracer.

ACKNOWLEDGMENTS

The author would like to express his gratitude to the following people who made the completion of this work possible:

To his director, Dr. D. Wolf, for his continual guidance and assistance during the course of this project.

To the Consolidated Mining and Smelting Company of Canada, Limited, for their award of a fellowship during the year 1965-66.

To the National Research Council of Canada for financial assistance in the purchase of equipment.

To Mr. D. Van der Merwe for his assistance and advice concerning the use of the hot wire anomemeter.

To the academic and technical staff of the Chemical Engineering Department, McGill University, for their invaluable help and guidance.

To my parents for their constant encouragement during the course of this graduate work.

TABLE OF CONTENTS

LIST OF ILLUSTRATIONS

LIST OF TABLES

INTRODUCTION

General

The purpose of this thesis was to study the velocity profiles and pumping capacities produced by various turbines in a stirred tank.

Until recently, much of the work done on impeller behaviour has been macroscopic in nature. In this respect considerable research has been concerned with power requirements, power dissipated in a mixer, and general flow patterns. To date the only common scale-up factor for mixers has been the power requirement.

The work on power requirements of various researchers, especially White and Brenner (1), Hixson & Baum (2), and Rushton et al. (3) has resulted in correlations and graphs relating the Power Number, N_{Po}, of a mixer to the Reynolds Number, N_{Re}, the Froude Number, N_{Fr}, various geometric shape factors and the properties of the system. The work in this field has been extensive, and these results are accepted today as standard methods for scaling-up a mixer.

Such a macroscopic approach cannot be used to predict such quantities as homogeneity of liquids in a blender, conversion in a continuous stirred tank reactor, residence time distributions and intensity of segregation in agitated tanks. We are therefore concerned in this work with what is occuring at a more basic level, such as the flow patterns in the vicinity of the impeller and the pumping capacities.

More work has been done in determining the flow patterns of propeller-type impellers than on turbine types. A correlation for pumping capacities for propellers has been found, and has the form:

$$Q = K_p N D^3 \qquad (1)$$

From the work on turbines, it is known that the fluid leaving the impeller forms a jet with two velocity components, a tangential and a radial component. A certain volumetric flow, namely the pumping capacity, passes through the impeller blades, and in doing so becomes completely mixed. Van de Vusse (4) has shown that the mixing time in a stirred vessel appears to be dependent on the pumping capacity of the impeller. Norwood and Metzner (5) have proposed that all mixing in a tank effectively takes place in the small volume occupied by the impeller, and that two streams entering the impeller zone are intimately mixed in the time it takes them to pass through the physical confines of the impeller. Therefore the volume through-put or pumping capacity of an impeller appears to be the chief criterion for mixing in an agitated vessel.

In the past, residence time distribution, intensity of segregation and concentration fluctuations have been measured for a stirred tank. While these quantities give an indication of the "goodness of mixing" in a tank, they cannot yet be predicted for a particular impeller, nor can they be scaled-up. It would appear that the ratio of pumping capacity to tank volume is a good scale-up parameter for mixing tanks.

Successful models have been proposed for the agitated tank using the pumping capacity as a parameter. In a simulation model of a continuous stirred tank reactor, proposed by Manning, Wolf and Keairns (6), the pumping capacity in addition to Danckwerts' segregation concept (7) and residence time distribution is used to calculate the degree of conversion for a second order reaction in an imperfectly mixed system. They use the pumping capacity of the impeller as a measure of the proximity of the system to the ideal mixing case. Cholette (8) also used the pumping capacity as a measure of mixing for developing a model of a non-ideal first order reaction system in much the same manner as Manning, Wolf and Keairns.

It was the purpose of this experimental work to develop an accurate, reliable and simple method of determining the velocity profiles around impellers, which can then be analyzed to give the pumping capacities. The turbine type was primarily investigated, but the method can easily be extended to other types of impellers. It was also an aim of this work to find correlations to predict the pumping capacities of turbines of different sizes and at various speeds.

Previous Experimental Methods

A considerable amount of data can be found in the literature on velocity profiles and pumping capacities of impellers. A great variety of experimental techniques are available. Much of the data is for marine propellers, where the flow is in the axial direction and is one dimensional, hence easier to measure.

In the case of the turbine impeller, as already mentioned, the jet formed in the horizontal plane, i.e. plane perpendicular to the axis, is two-dimensional flow, having radial and tangential components. Therefore to be able to obtain the pumping capacity, the magnitude of the velocity as well as the direction of flow is necessary.

Early developments in the field of pumping capacities included the work of Rushton, Mack and Everett (9). They attempted to determine the pumping capacities of propellers and turbines by using two concentric tanks and measuring the flow displacement from one tank to the other produced by the impeller. This method of measuring total flow rather than point velocities appears to give results of the same order as those obtained by other researchers, but yields no information as to the velocity profiles and flow patterns of the impeller jet.

Sachs and Rushton (10) studied the velocity profiles of turbine using time exposure photography. Tracer particles were photographed in illuminated sections of the tank, and from the length of the streaks, the velocity was calculated.

Metzner and Taylor (11) also studied velocity profiles and shear rates of turbine jets by photographing tracer particles. The photographic method, however, is quite tedious, since the length of each tracer particle must be measured and its two velocity components determined. The illuminated slits are sufficiently wide so that a considerable velocity gradient occurs within each slit, and in effect, a width-average velocity rather than a point-velocity is measured.

Aiba (12) measured the velocity profiles of propellers, turbines and paddles by noting the deflection of a small suspended steel ball due to the viscous drag forces of the fluid in motion. The position of the radioactive ball was determined by using a geiger counter.

Norwood and Metzner (5) used an electrically heated thermistor probe to measure local velocities.

Porcelli and Marr (13), and later Marr and Johnson (14), used a "flow follower" technique for measuring pumping capacities of turbines. A neutrally buoyant flow follower was observed as it circulated throughout the tank; the number of times it passed through the impeller blades in a period of time was used to calculate the recirculation time and the pumping capacity. However, this method gives no information about velocity profiles.

Holmes, Voncken and Dekker (15) describe a method for measuring pumping capacities and velocity profiles using a 15 mm. miniature propeller flowmeter. The recirculation times of the contents of the tank were measured by a tracer pulse injection technique. The time for the tracer to become mixed with the contents of the tank was measured with a conductivity cell. Nothing was reported about the possibility and accuracy of measuring the direction of flow and flow components using the propeller flowmeter.

Wolf and Manning (16) used a shielded impact static tube to measure the velocity profiles in the jets of propellers and turbines. The method proved effective, but no quantitative

results were reported for the turbine type impellers.

Cutter (17) measured the velocity profiles and pumping capacities of turbines using both the photographic method and a Kiel impact tube. There was good agreement between the two methods. However, because of the insensitivity of the Kiel tube to the yaw angle, information on the direction of flow could not be obtained with it.

In review, the most accepted method for quantitative measurement of velocity profiles in a turbine jet is the photographic technique. However, this method is time-consuming, and to obtain point velocities, the illuminated slits must be extremely narrow, which becomes impractical.

The present work uses three methods of velocity measurement and flow pattern determination: two and three dimensional pitot tubes, a hot wire anemometer, and a smoke generation technique. In this work it is possible to measure velocity and angle of flow profiles across the turbine with greater ease and simplicity. The feasibility of using a pitot tube in a turbulent regime and its accuracy have been discussed in detail by Wolf and Manning (16). The calculated error for 20% turbulence was found to be 2%.

THEORETICAL

Much of the work done in the field of pumping capacities has been empirical, and analytical approaches to the problem are few.

The propeller pumping capacities are correlated by the empirical formula $Q = K_p ND^3$, where the values of K_p reported by a number of researchers lie in the range of 0.4 to 0.6. This correlation can be expected by noting that the pumping capacity is a function of the product of the blade tip velocity (πDN) and the projected area ($\pi D^2/4$). This gives the pumping capacity as:

$$Q = K_p ND^3 \qquad (1)$$

where K_p is some constant which relates the axial velocity to the blade tip velocity. However, using a more analytical approach as developed in Appendix I, the theoretical pumping capacity obtained is equal to $K_p ND^3$ where K_p is a function of the propeller pitch and shape. For a pitch of 30°, the calculated theoretical K_p for a three blade propeller is 0.96, and for 45° it becomes 1.65.

For turbine type impellers, Van de Vusse's (4) analytical development was as follows: he considered the turbine impeller as being similar to the radial flow or centrifugal pump. Using the concept of Euler's head or lift, he proposed a force or head balance over the turbine. His expression for pumping capacities of turbines in baffled tanks is:

$$Q = \pi^2 ND^2 W \qquad (2)$$

The work of Norwood and Metzner (5) showed that the

coefficient relating Q to ND^2W was in fact not a constant, as Van de Vusse's development predicts. Neilson (18) also verified this conclusion.

Holmes, Voncken and Dekker (15) assumed that the average radial velocity was proportional to the blade tip velocity πDN; the flow area is πDW, where W is the width of the blade. Therefore the pumping capacity is:

$$Q = K_{t1}ND^2W \qquad (3)$$

$$\text{or} \quad Q = K_{t2}ND^3 \qquad \text{if W/D is constant.}$$

Their equation is of the same form as Van de Vusse's, but they substitute K_{t1} for π^2 in Van de Vusse's equation.

In measuring velocity profiles of turbines, Sachs and Rushton (10) found that the shapes of the velocity profiles were independent of impeller speed. Aiba (12) also verified this, and was even successful in correlating power consumption and flow patterns. Metzner and Taylor (11) found that local velocities in the discharge jet were proportional to the turbine rotational speed.

Using data available from the work of these researchers, the values of K_{t2} were calculated from equation 3. These values are tabulated in Table I, and can be compared to the value of K_{t2} of 1.3 as reported by Holmes et al. (15).

TABLE I. Calculated Values of K_{t2}

References	Turbine Diameter	No. of Blades	Calculated K_{t2}
Cutter* (17)	4"	6	1.4
Sachs and Rushton (10)	4"	6	0.47
Rushton et al. (9)	6"	6	0.6
Holmes et al. (15)	4"	6	1.3

*Cutter used the total or resultant velocity rather than the radial component to calculate the pumping capacity. This point will be discussed in more detail in a later section.

In the analytical approach which is outlined in detail in Appendix II, the radial velocity profile across the width of the blade is given by:

$$V_R = C_1 \omega R \cot\left[\frac{z}{2C_1^2 R} + \frac{\pi}{4}\right] \qquad (4)$$

where C_1 is a coefficient in the range: $0.614 \leq C_1 \leq 0.707$. This expression is valid for positive values of z, where z = 0 is the centre-line of the turbine. If this expression is integrated across the width of the blade and multiplied by the turbine circumferences, the resulting expression for the pumping capacity is:

$$Q = 2\pi^2 D^3 C_1^3 \cdot \ln\left(\sqrt{2} \sin\left[\frac{W}{2C_1^2 D} + \frac{\pi}{4}\right]\right) \qquad (5)$$

and for the usual dimension of W/D = 1/5

$$Q = K_{t2} N D^3 \qquad \text{where } 0.946 \leq K_{t2} \leq 1.17$$

$$\text{and } Q = K_{t1} N D^2 W \qquad \text{where } 4.73 \leq K_{t1} \leq 5.85$$

EXPERIMENTAL

In this section, the apparatus is described followed by the experimental procedure and measuring techniques.

Apparatus

Most velocity measurements were made in a 10 Imperial gallon clear acrylic tank, as shown in Figure 1. The baffled tank measured 15" in diameter and 20" in height. Each of the four baffles were $1\frac{1}{2}$" in width.

Several velocity measurement probes were used:

(i) a hot wire probe for air, and

(ii) two and three dimensional pitot probes for liquids.

In this manner it was hoped that the results from different measurement techniques (hot wire and pitot tube) and different fluids (air and water) could be compared.

The constant temperature anemometer used was manufactured by the Disa Electronik Corporation. The particular model used was 55A01, which gives voltage readings of the time-averaged velocities. The hot wire probes used for velocity measurement in air were also manufactured by the Disa Electronik Corporation, and had a wire diameter of 5 μm. The time constant for the probe and anemometer was less than 0.01 sec. The hot wire probes were calibrated in a round-edged orifice, where the flow can be assumed to be plug flow. The volume flow rate of air passing through the calibration orifice was measured by a rotameter. Figure 2 shows the calibration unit.

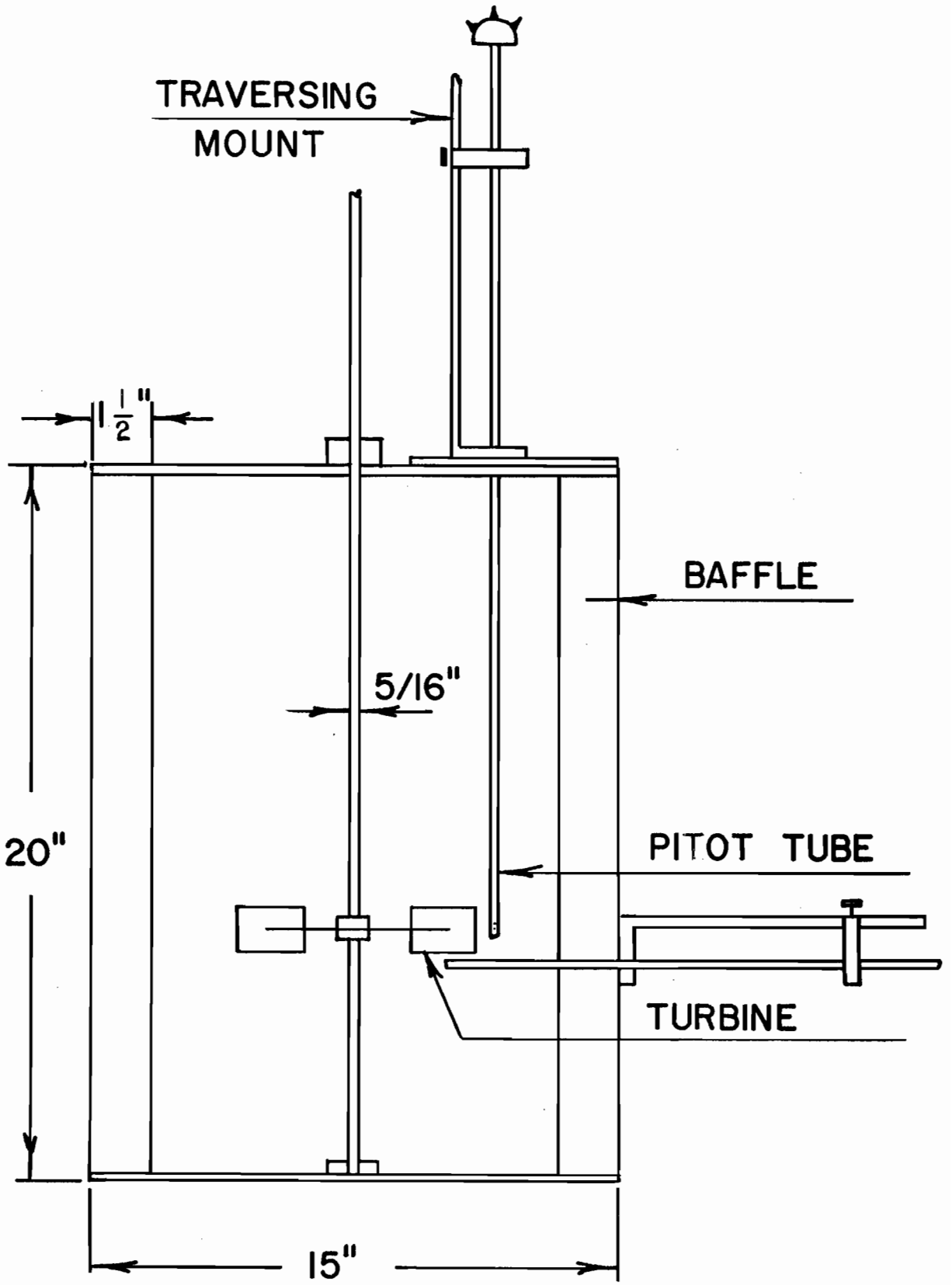

FIGURE 1 : STIRRED TANK AND TRAVERSING UNIT

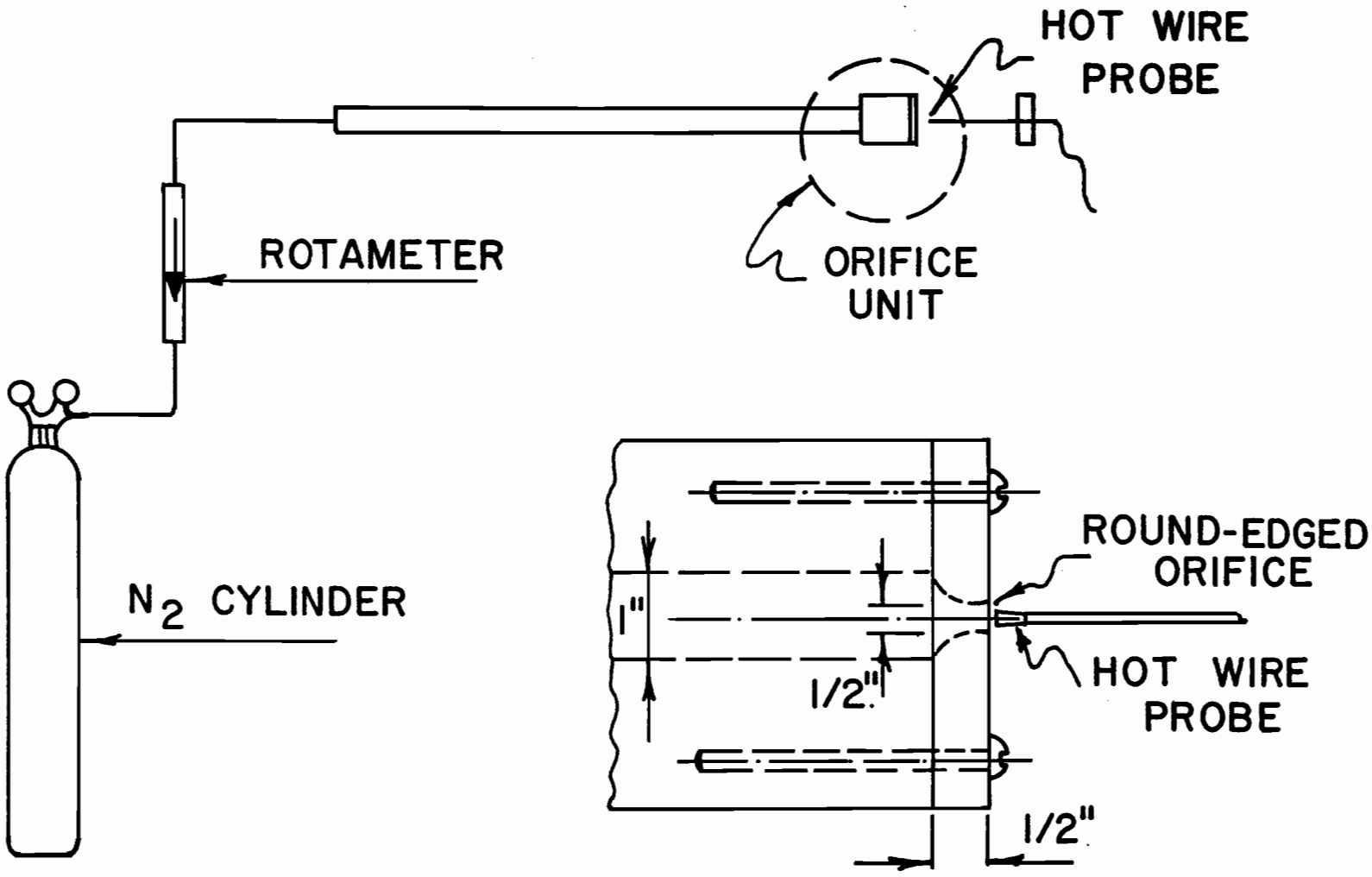

FIGURE 2 : CALIBRATION ORIFICE FOR HOT WIRE PROBES

The two and three dimensional pitot probes used were models YC125 and DA125, manufactured by the United Sensor Corporation. A sketch of the two dimensional probe is shown in Figure 3. The sensing end of the probe measures 1/8" in diameter; the pressure taps were located on the wedged section of the probe. The centre pressure tap, P_1, gives the total pressure, while the side taps, P_2 and P_3, on the opposite sides of the wedge, give the static pressure.

The three dimensional probe was identical in construction to the two dimensional probe with an additional two pressure taps located on the point of the wedge above and below the total pressure tap, P_1. The United Sensor Corporation provided calibration curves for correcting static pressures and determining the pitch angle from pressure readings for the three dimensional probe.

These probes were ideal for measuring time-averaged velocities in the discharge jet of the turbine. Usual pitot tubes are L-shaped, and when rotated, the total pressure tap traces out an arc. Since the probes used had pressure taps located on the axis of rotation, the point velocity measured remained on the same axial line. The static pressure, P_2 and P_3, measured by the side pressure taps, were extremely sensitive to angle of rotation and the angle could be effectively measured with an accuracy of one-half of a degree.

A probe traversing unit was mounted on the lid of the tank on a sliding mount for vertical traverses. The sliding

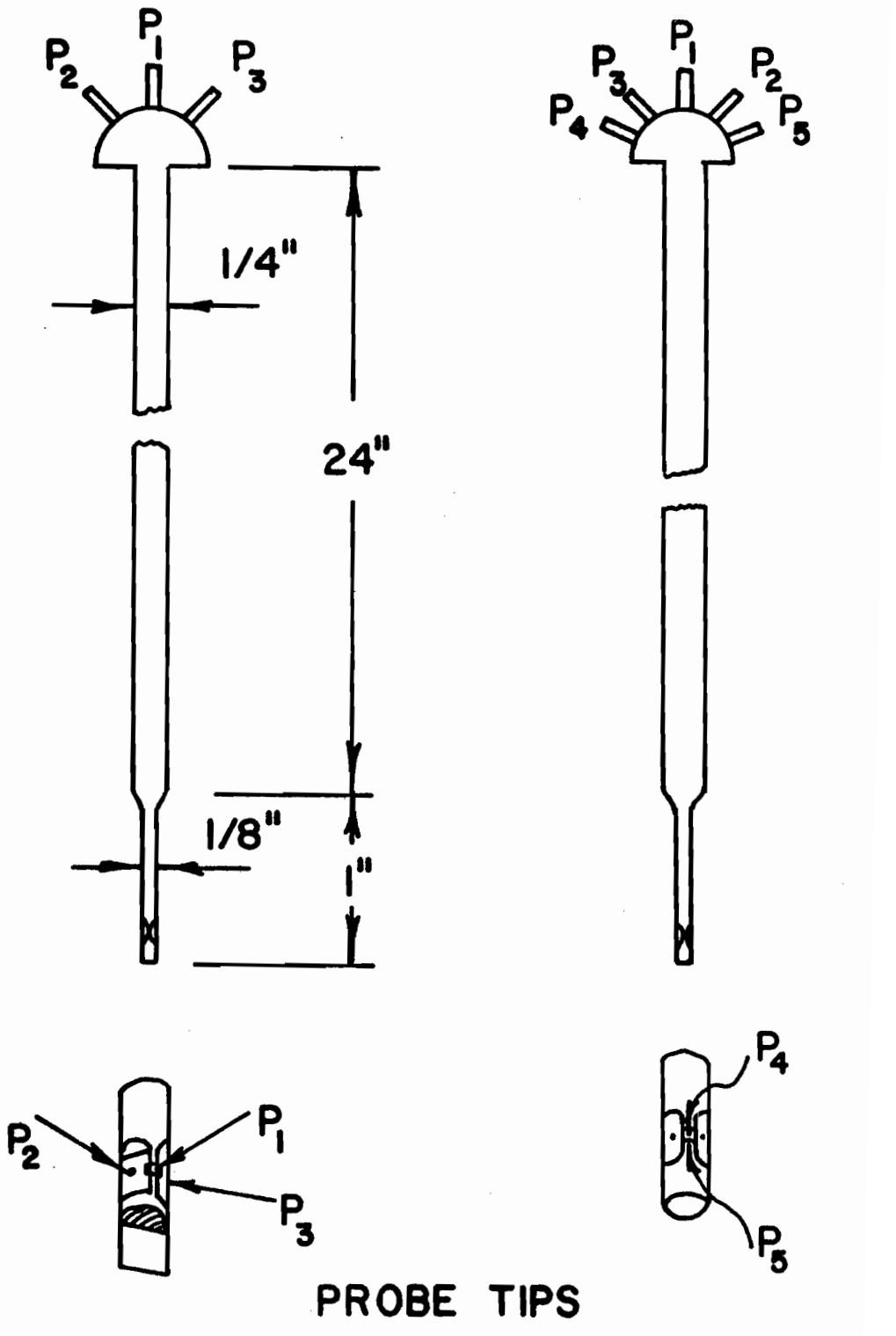

FIGURE 3 : TWO AND THREE DIMENSIONAL PITOT PROBES

mount permitted measurements at different radial distances. The traversing unit, vertically mounted, measured the depth of insertion of the probe to the nearest 1/100th of an inch on a vernier scale, and also the angle of rotation. This traversing unit could also be mounted on the side of the tank for horizontal traverses. A water-tight seal prevented leakage of the liquid from the tank where the probe passed through the tank wall. Details of the traversing unit are shown in Figure 1.

The smoke generator used to detect the general flow patterns around the impeller, is shown in Figure 4. The smoke was obtained by passing a stream of air through a smoldering bed of tobacco soaked with heavy oil.

In this work, propeller type and flat blade turbine type impellers were studied. In the case of propellers, an 8" three blade marine propeller and a 10" four blade axial flow fan were investigated. Most of the turbines studied had six blades and were geometrically similar, having a D:W:L ratio of 20:4:5. Figure 5 shows the two types of impellers studied, and Table II lists the impeller dimensions.

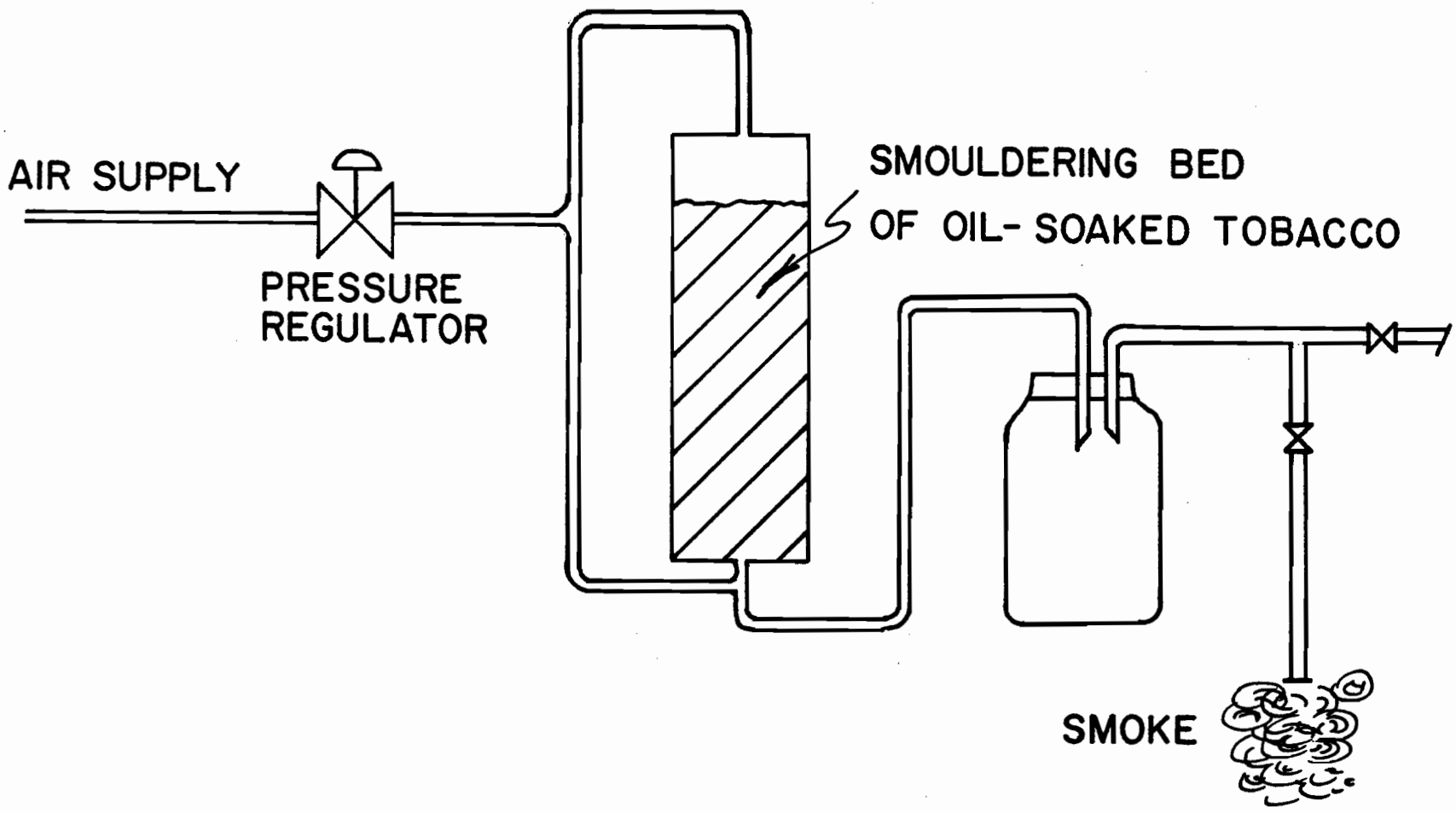

FIGURE 4 : SMOKE GENERATOR

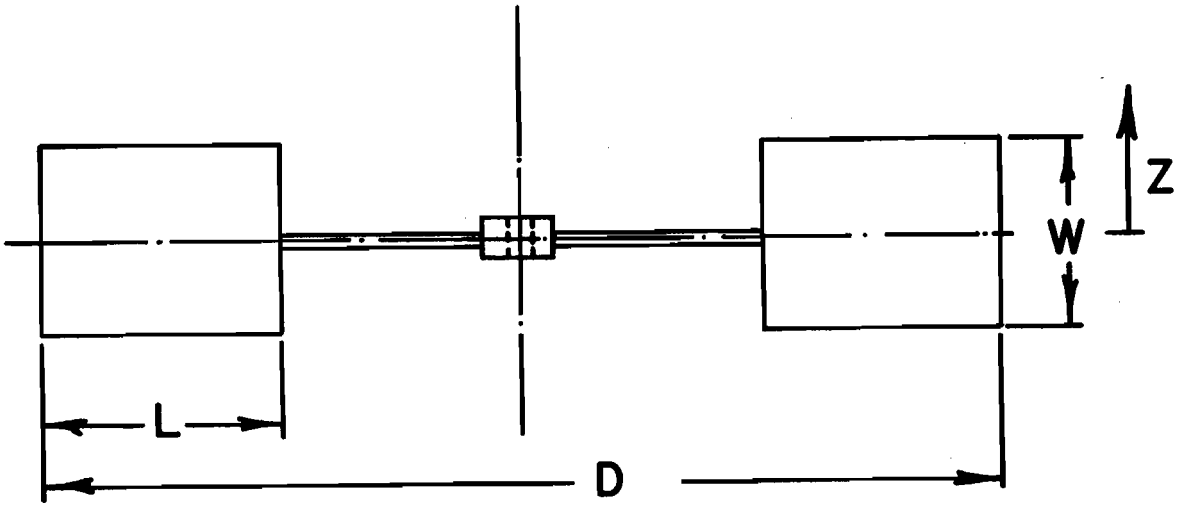

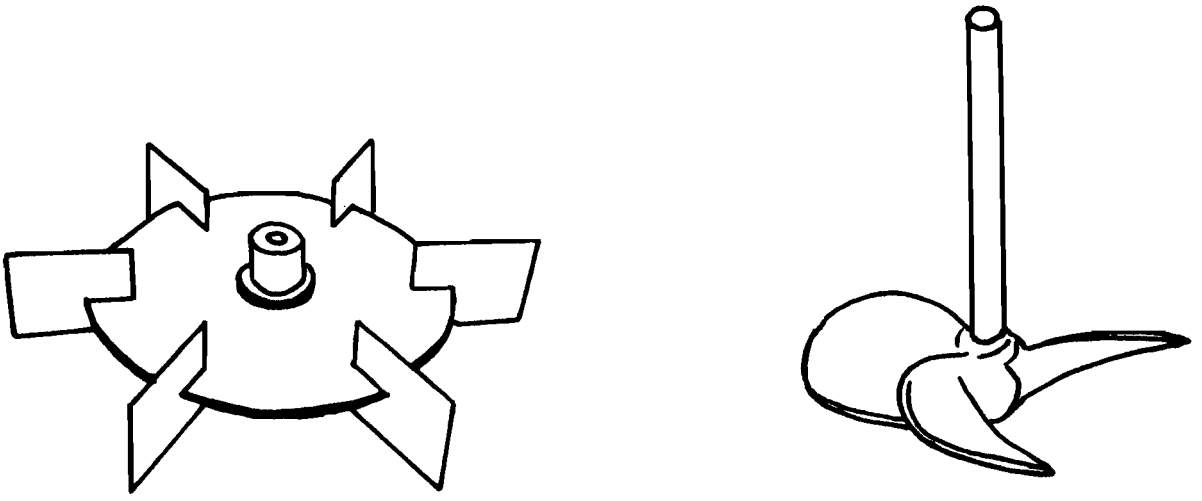

FIGURE 5 : TURBINE TYPE AND PROPELLER TYPE IMPELLERS

TABLE II. Turbine Impeller Specifications

Turbine No.	Diameter in.	Blade Width in.	Blade Length in.	No. of Blades in.
1	3	0.6	0.75	6
2	4	0.8	1.0	6
3	5	1.0	1.25	6
4	6	1.2	1.5	6
5	9	1.8	2.25	6
6	9	3.6	2.25	6
7	4	0.6	1.0	6
8	4	1.0	1.0	6
9	4	1.2	1.0	6
10	4	1.4	1.0	6
11	4	1.6	1.0	6
12	4	0.8	1.0	10

Procedure

To measure the velocity profiles of the discharge flow from the turbines, traverses were made in the vertical, i.e. z direction across the width of the turbine blades. The probes, either hot wire or pitot tube, were placed as close as possible (less than 1/10") to the blade. This was done in order to measure the velocities at the blade tips, eliminating the entrainment effect in the discharge jet.

Point velocities and angles or directions of flow were measured at increments of 1/10" across the width of the blade, except in the case of the 3" turbine, where measurements were made at 1/20" increments. The vernier scale on the traversing unit was useful for obtaining the vertical position of the probe.

The pitot tube was rotated until the two side pressure taps gave identical readings indicating that the flow was normal to the cross section area of the total pressure tap. Using this pitot tube, a velocity magnitude and direction was determined for each z position. In this way, a velocity profile and angle profile were obtained across the width of the blade.

In using the hot wire, the probe was rotated until a maximum velocity reading was obtained, and so the flow direction and magnitude were determined. The angles of flow observed by this method were in agreement with those obtained using the two dimensional pitot tube. However, since the pitot tube was more sensitive to the direction of flow compared to the low sensitivity to the angle of the hot wire probe, the angle profiles as measured by the pitot tube are reported, and were used to calculate the radial and tangential flow components obtained in both methods of measurement.

To measure the velocity profiles of the axial flow intake to the turbine, and the axial discharge flow from the propeller, horizontal traverses were made along the radius of the impeller. In the case of turbines, the probe was positioned close to the turbine (1/10"), while measurements were made at a

distance of $1\frac{1}{2}$" from the propeller. For water, the three dimensional pitot tube was used, and the readings were corrected for pitch angle using the calibration curves supplied by the manufacturer. The hot wire probe was used for velocity measurements in air, and using the directional information obtained by the pitot probes, the necessary corrections for the pitch angle were made. Because of the relatively lower velocities obtained in the axial direction compared to discharge velocities, the hot wire results were considered more accurate due to its higher sensitivity at low velocities.

Using the above techniques, velocity measurements were made at different rotational speeds, with different sizes of impellers and at various radial distances.

The qualitative evaluation of the flow patterns using the smoke generator were obtained by injecting the smoke at different locations around the impeller and observing the stream of smoke entering and leaving the impeller.

RESULTS AND DISCUSSION

The previous section outlined the experimental technique and the equipment used to study the fluid velocities in a stirred tank. This section will present the experimental results and a discussion of their implications.

Evaluation of Experimental Technique

Initially it was desired to check the reliability of the two methods of measurement used, particularly in the case of the pitot probes. For this purpose it was decided to compare the pumping capacities of propellers to the results available in the literature, and also to carry out material balances over the turbine.

By using the two dimensional probe in a horizontal traverse across the 8" marine propeller, the pumping capacity coefficient K_p for water, was found to be 0.53 ± 0.03 for a range of impeller speeds of 200 to 300 R.P.M. Using the same propeller with air as the fluid, the hot wire probe gave a K_p value of 0.52 ± 0.01 for speeds of 200 and 300 R.P.M.

These experimental values of K_p agreed closely with the results reported so far, in the range 0.4 to 0.6 and were of the same order of magnitude as the theoretical values obtained in Appendix 1. These previously reported values were obtained for a variety of propeller types and using different measuring techniques. It is also interesting to note that the fluid used in this work had little effect on the value of K_p. These results are reassuring and

lend confidence to the experimental techniques. They also help to substantitate the value of K_p of 0.54 as reported by Wolf and Manning (16) using an impact static shielded tube.

In an attempt to determine the consistency of experimental results, several material balances were conducted over the turbine for the air and water cases. For air, a 9" turbine with a speed of 420 R.P.M. was used. The pumping capacity determined from a vertical traverse across the blade width was 156 cu.ft./min., while the pumping capacity from a horizontal traverse across the face of the turbine was 153 cu.ft./min., which gives an agreement to within 2%. For water, the 4" turbine rotating at 300 R.P.M. was used. The pumping capacities as found by the vertical and horizontal traverses were 7.97 and 8.50 cu.ft./min. respectively, also indicating consistent measurements. Here the results differed by 6.3%; this higher discrepancy was attributed to the lower sensitivity of the pitot tube at the lower velocities across the turbine face.

Velocity Profiles with Geometrically Similar Turbines:

Local fluid velocities and inclination of flow were measured at different vertical, i.e. z positions in a traverse across the width of the turbine blade, using pitot tubes for water and hot wire probes for air. The two dimensional pitot tube was used after the existence of two dimensional flow was verified by the three dimensional pitot tube. The pitch angle detected was negligible. A variety of geometrically similar turbines were used, each at five different rotational speeds.

Unless otherwise mentioned, the turbine dimensions were D:W:L = 20:4:5.

From the point velocities and directions of flow, the radial and tangential velocity profiles were determined. Appendix V summarizes the velocity and angle profile data obtained. Figures 6 and 7 present the velocity profiles for the radial, tangential and resultant velocities for both water and air as fluids. These curves give a good representation of the nature of flow in the jet leaving the turbine. The radial component profile in both cases has a parabolic shape; the tangential profile is flatter in shape, indicating that the flow becomes more radial as one approaches the centreline of the turbine. The flatter tangential profile is to be expected, if the fluid within the turbine blades is assumed to move at the blade angular velocity. The ideal condition assumed in the theoretical development was a completely flat tangential velocity profile, with the fluid rotating at the same angular velocity as the turbine. The end effects existing in the experimental tangential profile obtained, and the angle profiles will be discussed later.

Figures 8 and 9 show the radial velocity profiles for liquid and air for the 4" turbine at the indicated speeds. The curves are typical of the velocity profiles obtained where geometrically similar turbines were studied in the course of this investigation.

Sachs and Rushton (10) and Aiba (12) showed that the shape of the radial velocity profile was independent of speed.

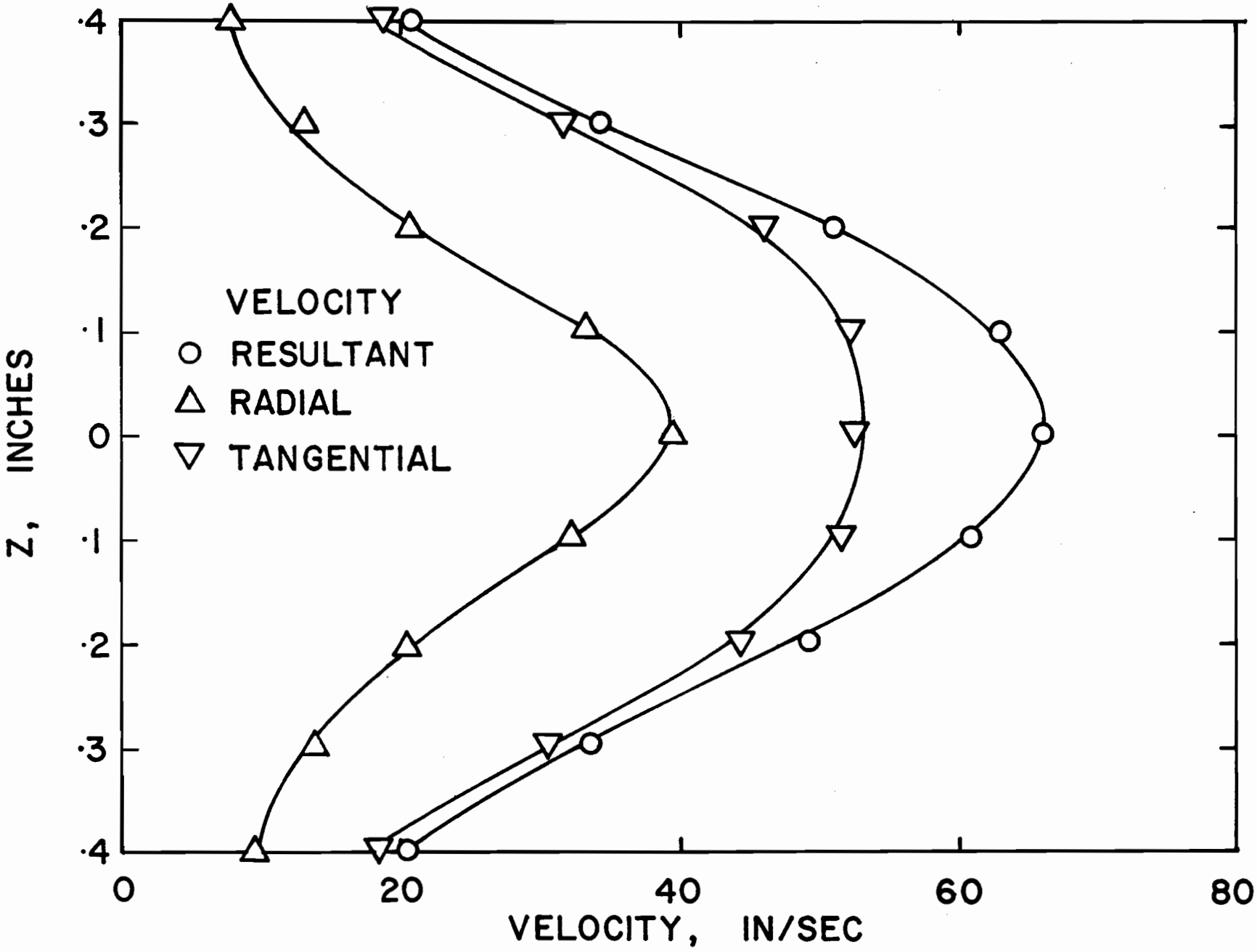

FIGURE 6 : RADIAL, TANGENTIAL AND RESULTANT VELOCITIES FOR 4" TURBINE IN WATER

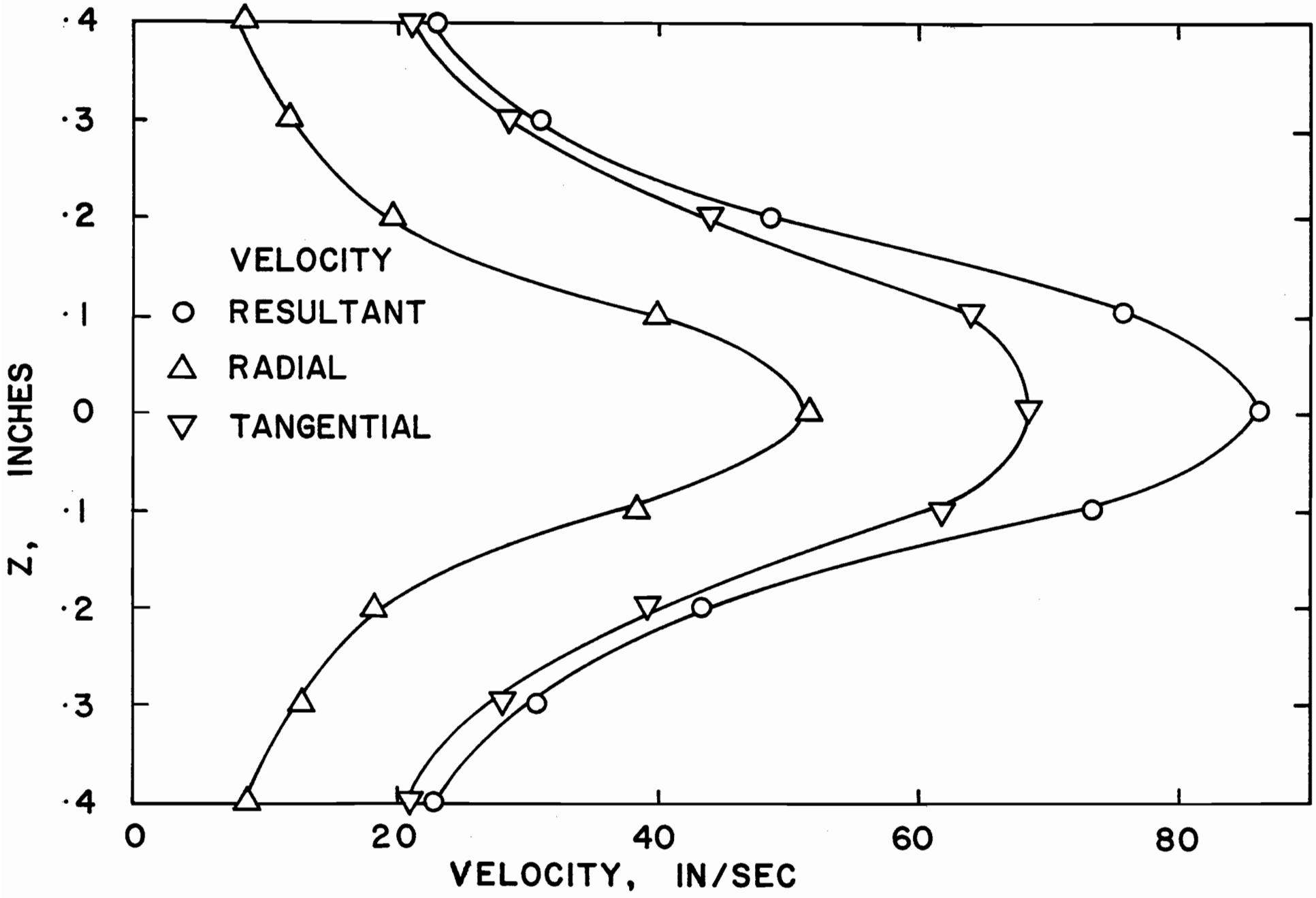

FIGURE 7 : RADIAL, TANGENTIAL AND RESULTANT VELOCITY PROFILES FOR 4-INCH TURBINE IN AIR

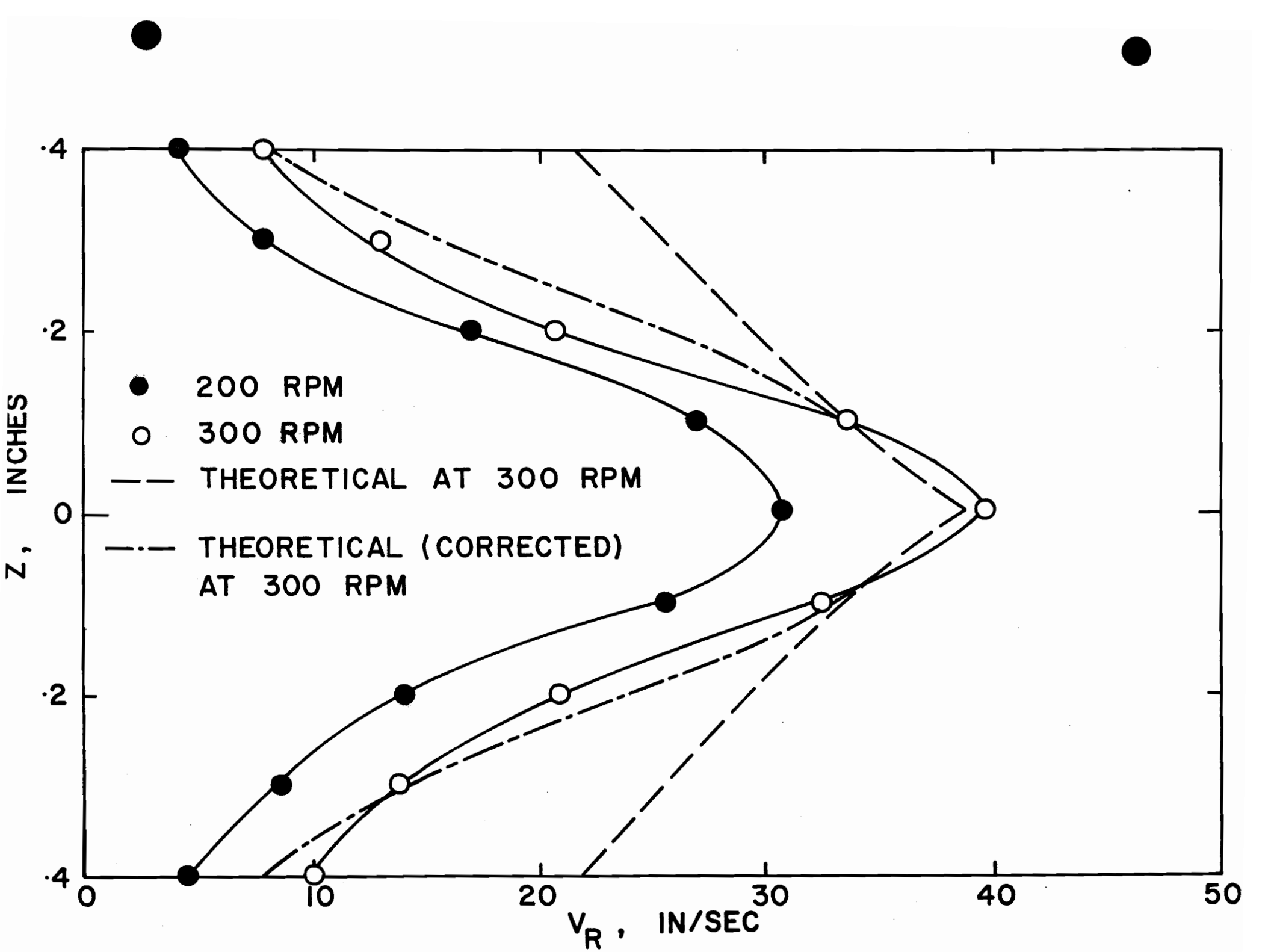

FIGURE 8 : RADIAL VELOCITY PROFILES FOR 4" TURBINE IN WATER

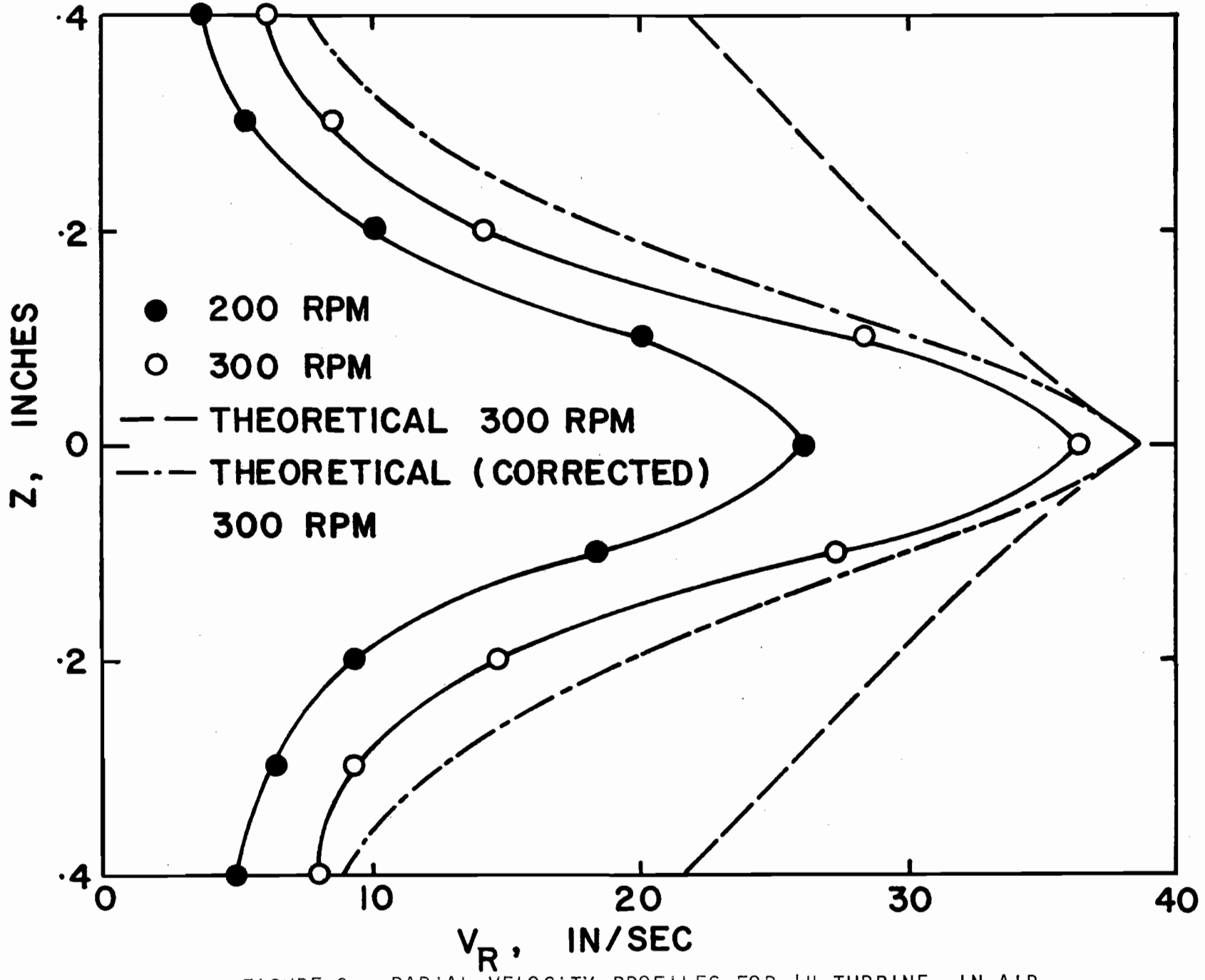

FIGURE 9 : RADIAL VELOCITY PROFILES FOR 4" TURBINE IN AIR

Figures 10 and 11 verify their conclusions. The normalized radial velocity, taken as the ratio of the point velocity at some vertical position z, to the centreline radial velocity, is plotted against the vertical position z. At different rotational speeds, almost identical curves are obtained for a given turbine, indicating that the curve shape is independent of speed. Figures 10 and 11 are typical normalized velocity profile curves. Figures 12 and 13 show several normalized radial velocity profile curves, with the vertical dimension also normalized, indicating how the shape of the profile is independent of turbine size for geometrically similar turbines.

The consistency of the experimental values obtained by this technique is well demonstrated by the low degree of scatter of points in these velocity profile curves. Although not all the curves are shown here, this was found to be so in all experimental cases. One can see that the velocity gradient in the vertical, i.e. z direction, is high, and that measurement of point velocities rather than width-averaged velocities is essential.

Referring to the velocity profiles of Figures 8 and 9 the dashed lines indicate the profiles calculated from the theoretical equation developed:

$$V_R = 0.614\,\omega\, R \cot\left[\frac{4z}{3R} + \frac{\pi}{4}\right] \qquad (4)$$

where $C_1 = \sqrt{1/2(1 - k^2)}$ $\qquad 0 \leq k \leq 1/2$

$C_1 = 0.614$ if $k = 1/2$

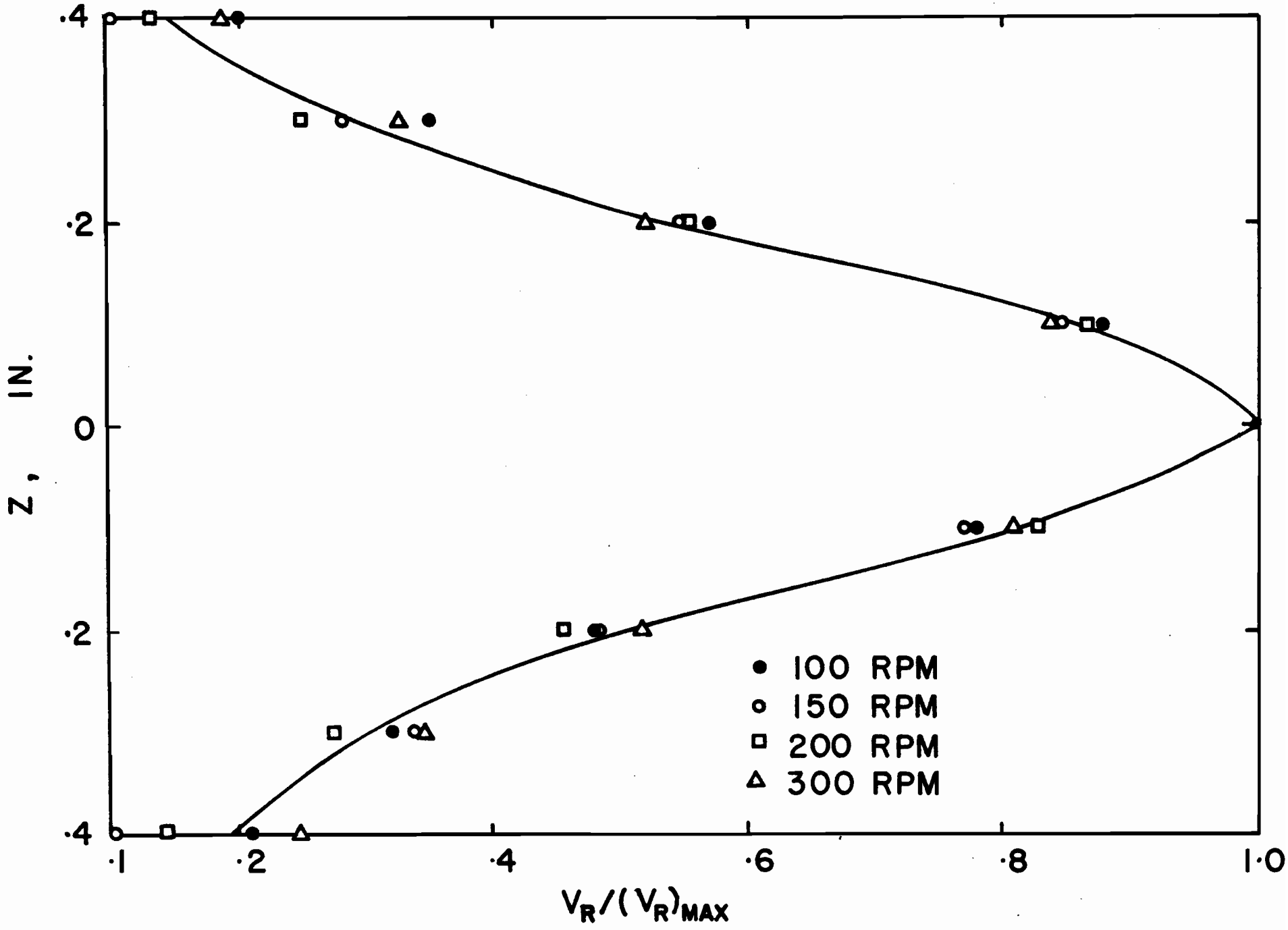

FIGURE 10 : NORMALIZED RADIAL VELOCITY PROFILES FOR 4" TURBINE IN WATER

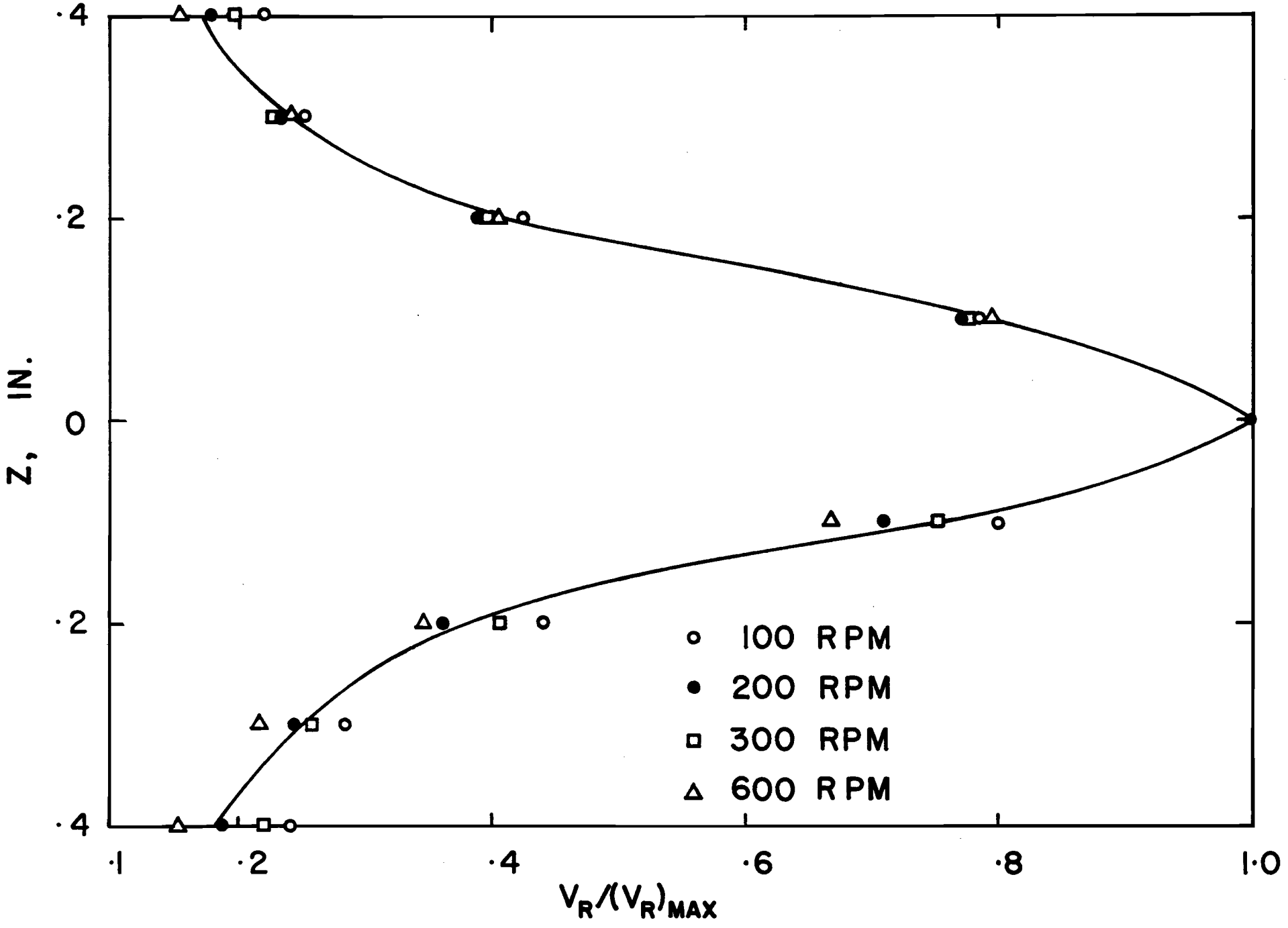

FIGURE 11 : NORMALIZED RADIAL VELOCITY PROFILES FOR 4" TURBINE IN AIR

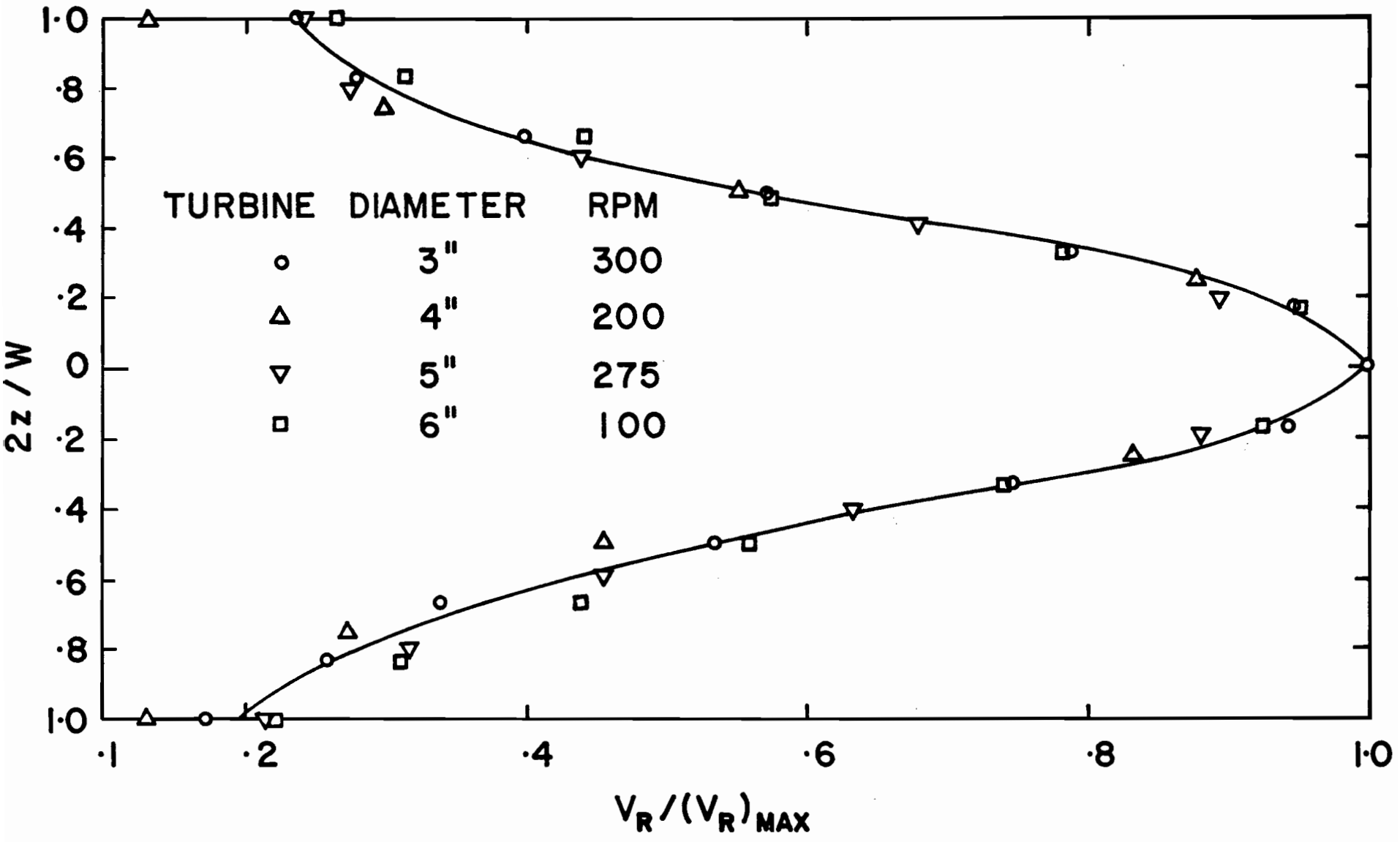

FIGURE 12 : NORMALIZED RADIAL VELOCITY PROFILES FOR VARIOUS TURBINE SIZES IN WATER

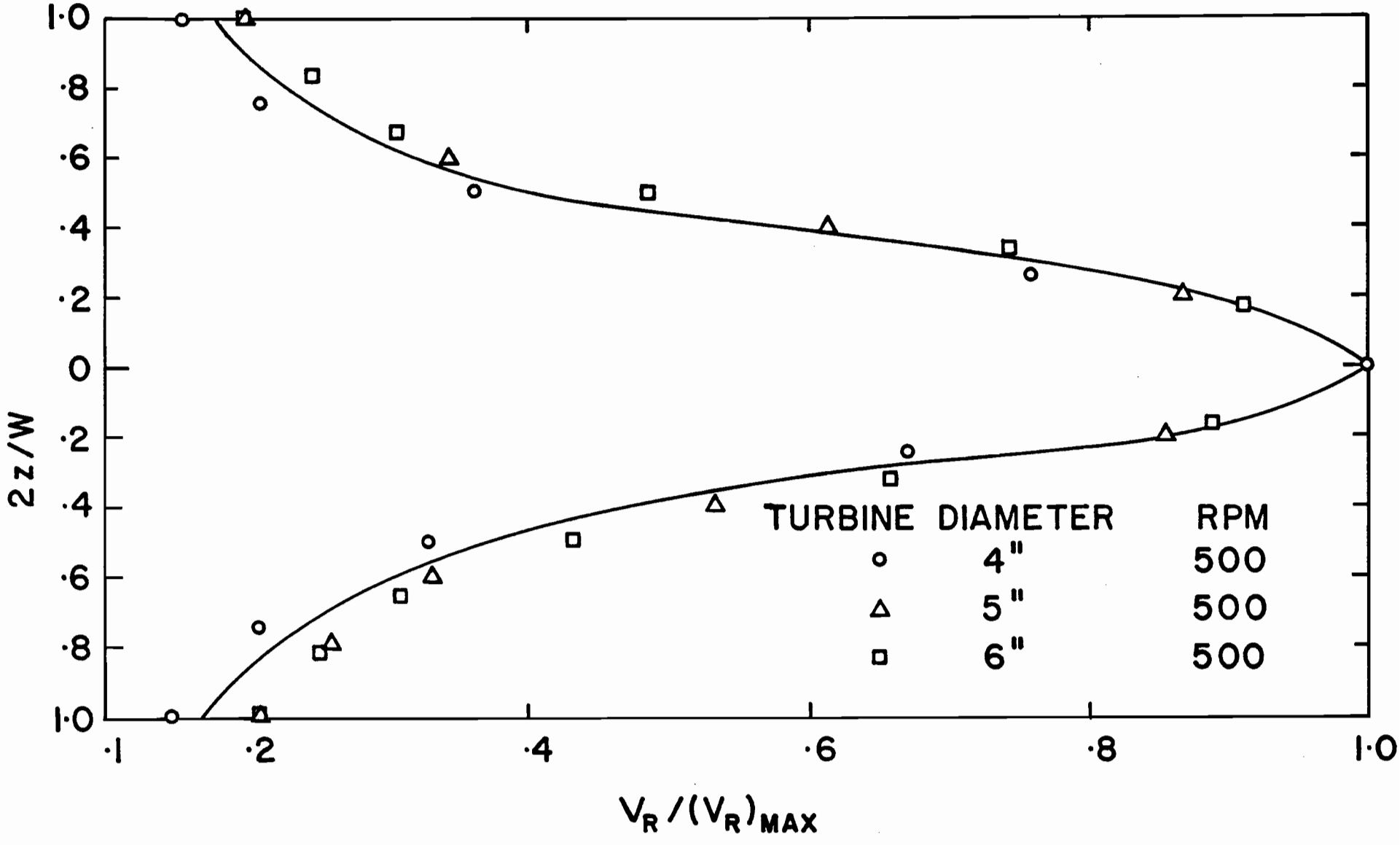

FIGURE 13 : NORMALIZED RADIAL VELOCITY PROFILES FOR VARIOUS TURBINE SIZES IN AIR

Here the model parameter k, as defined in the theoretical development, was chosen to be 1/2; the curve changes very little if k is chosen to be zero.

The theoretical model predicts the maximum velocity at the centreline ($z = 0$) quite accurately and indicates the general shape of the curve. The most serious differences between the experimental and predicted values of radial velocities occur as one approaches the top and bottom of the blades. The values obtained from the theoretical equation are somewhat higher than the experimental values. This is due to the assumption that the liquid within the confines of the turbine blades has the same angular velocity as the turbine. Figures 6 and 7 indicate that although the tangential velocity is flat for part of the blade width, at the outer edges the fluid rotates at a considerably lower angular velocity. Apparently closer to the blade edges, fluid leaves the turbine system before it has been accelerated by the blades to the blade angular velocity. Correcting the value of ω by multiplying the turbine velocity by the ratio of the tangential velocity at z to the tangential velocity at the centreline, as shown in the following equation:

$$V_R = 0.614\omega' R \cot \left[\frac{4z}{3R} + \frac{\pi}{4} \right] \qquad (4)$$

where ω' = fluid angular velocity

ω' = turbine angular velocity $\times \dfrac{\text{tangential velocity at z}}{(\text{tangential velocity})z = 0}$

the calculated radial velocity profile obtained was very close to the experimental profile, as shown in Figures 8 and 9. It is

also significant that the velocity profiles for both air and water differ very little, even though the fluids have widely different physical properties.

Since the shape of the velocity profile curves for geometrically similar turbines is the same, the value of the maximum velocity of the profiles is of special interest. Values of the maximum or centreline radial velocity have been plotted against rotational speed for geometrically similar turbines in Figures 14 and 15. The slopes of the straight lines obtained in these figures give values of C_1 between 0.58 and 0.75, which are close to the predicted values of 0.614 to 0.707 obtained from the theoretical equation.

Direction of Flow

As explained in the experimental procedure, the two dimensional pitot tube was used to measure the angle of the resultant velocity in the turbine jet. To obtain an accurate angle of flow appeared to be the main problem in using pitot tubes for measuring flow in a turbine jet. Cutter (17) reports the use of a Kiel-impact tube, and Wolf and Manning (16) used an impact-static-shielded tube. Both realized the fact that an angle profile existed, but were unable to measure it quantitatively. However, Wolf and Manning reported a range of angles for the flow in the discharge jet.

In this work the angle profile was obtained, and velocity components could be calculated. The angle of flow θ, varied between 70° and 48° for geometrically similar turbines (θ is zero

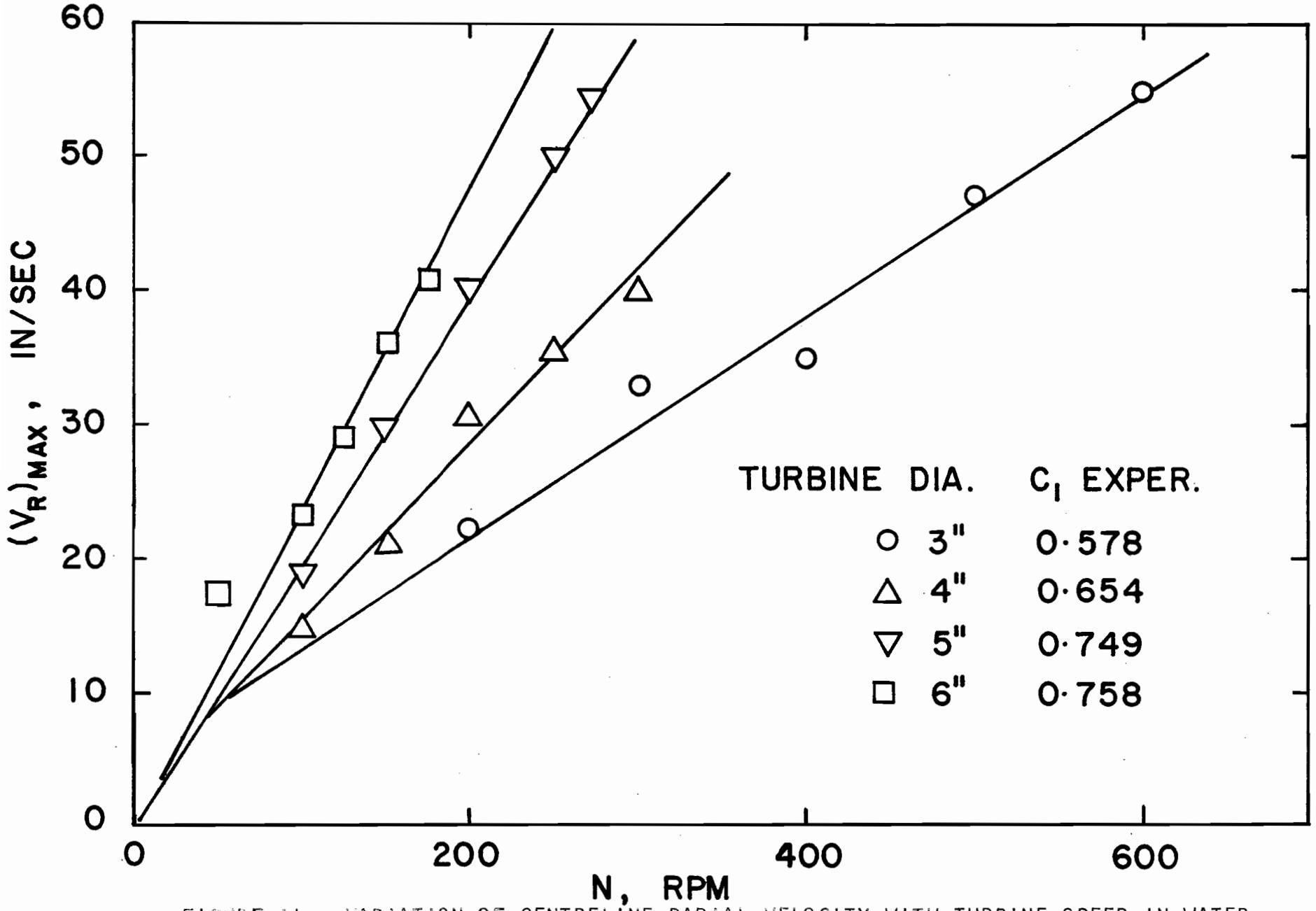

FIGURE 14 : VARIATION OF CENTRELINE RADIAL VELOCITY WITH TURBINE SPEED IN WATER

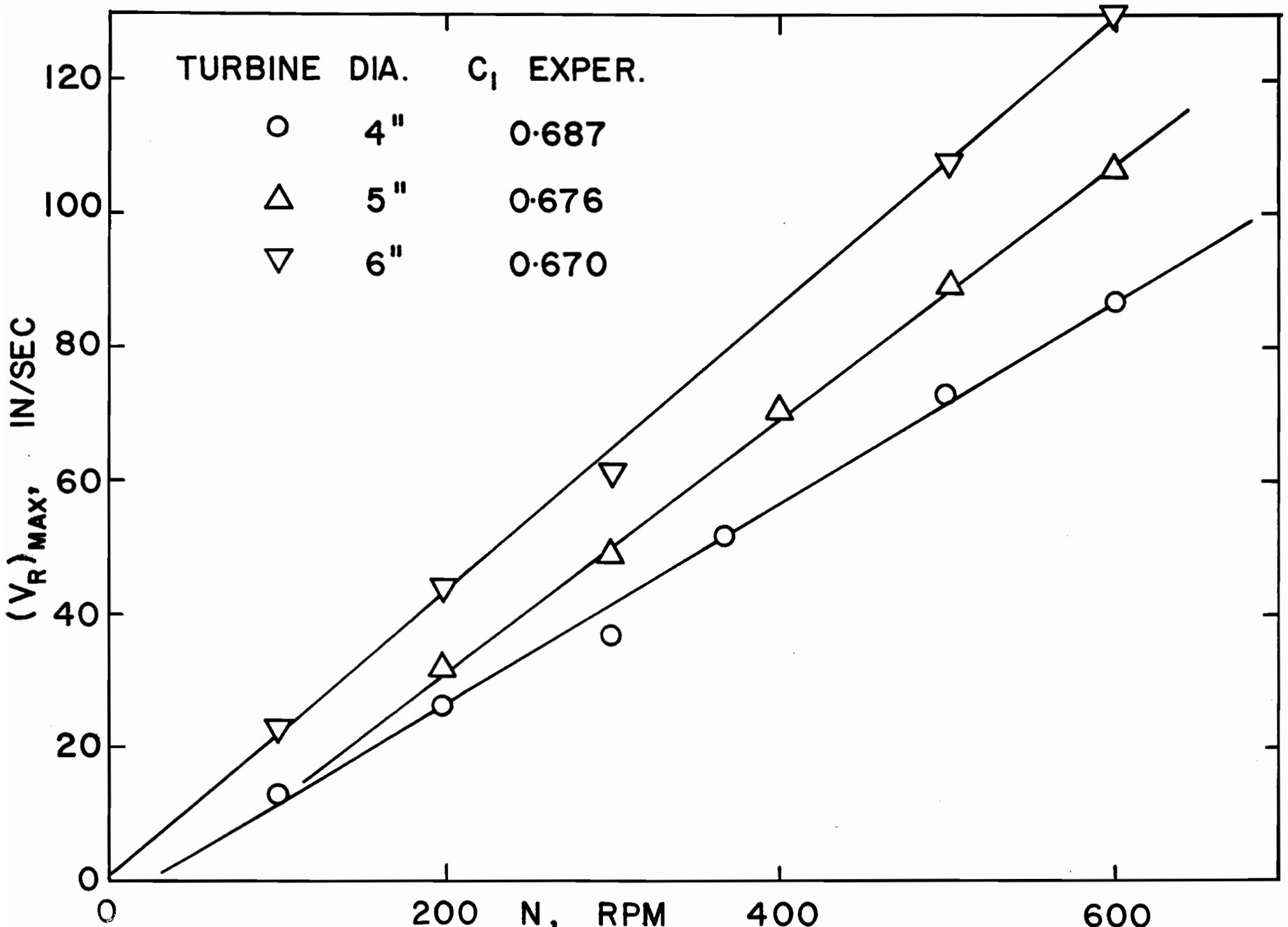

FIGURE 15 : VARIATION OF CENTRELINE RADIAL VELOCITY WITH TURBINE SPEED IN AIR

for pure radial flow). At the outer extremes of the blades, a value of 70^{o} indicates that the flow here is mostly tangential.

Figure 16 shows a plot of the angle of flow versus the vertical distance from the centreline, z, for the 4" turbine. Most of the flow lies in the range of 50^{o} to 60^{o}, as is the case with the other geometrically similar turbines studied. Towards the centreline of the turbine, the flow becomes more radial in direction. Like radial velocity profiles, the angle of flow profile appeared to be independent of the turbine velocity, and also independent of the turbine diameter. These results, along with velocity measurements are tabulated in Appendix V.

This experimental data agrees with the theoretical development given in Appendix II, where the angle of flow obtained is:

$$\tan\theta = \frac{\tan}{C_1}\left[\frac{4z}{3R} + \frac{\pi}{4}\right] \qquad (6)$$

This equation predicts an angle of flow ranging between 55^{o} and 71^{o} across the blade width, showing no dependence on the turbine diameter or rotational speed.

Velocity Profiles at Different Radial Distances

To gain an insight into the flow patterns of the discharge jet as it leaves the region around the turbine, velocity measurements were made in the jet at different radial locations. A 4" diameter turbine was used, and measurements were made at radial distances of 2", 2.5", 3", 4", and 5". (Tank radius was 7.5").

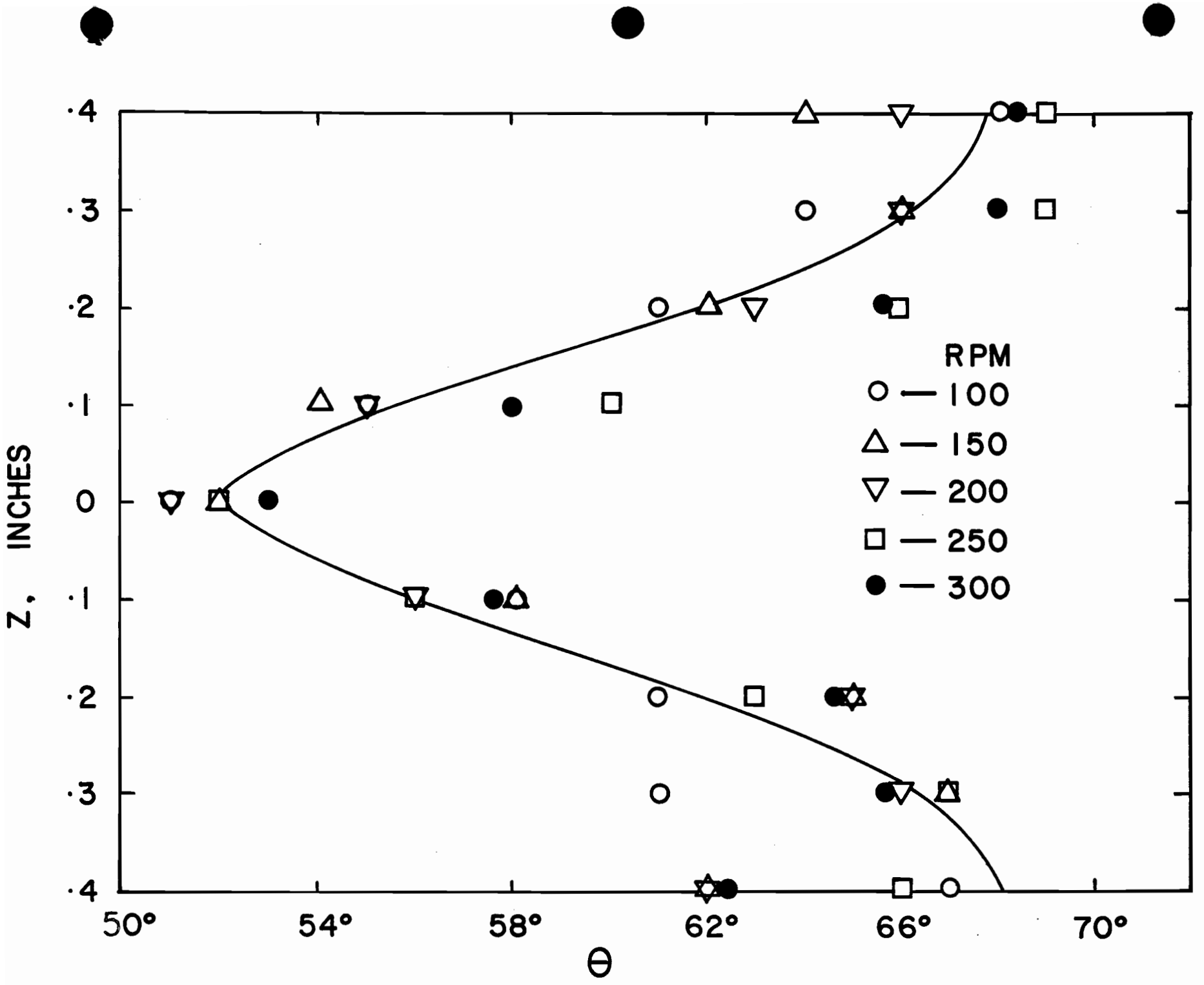

FIGURE 16 : ANGLE OF FLOW PROFILE FOR 4" TURBINE IN WATER

Sachs and Rushton (10) have showed that with increasing radial distances, the velocity profiles become more flat in nature. Velocity profiles are given in Figure 17 for the radial distances shown, and the trend to flatter profiles with increased radius is clearly indicated. The outermost velocity profile at a radial distance of 5" is evidently affected by the proximity of the tank wall, and hence gives an almost plug-shaped profile. Appendix V gives a tabulation of the velocities obtained. Figure 18 shows how the direction of flow changes with radial distance. It is significant that the flow becomes more radial with increasing radial distance. This is so because of the geometry of the system which indicates that θ decreasesas the radial distance increases as shown in Appendix III, and also because of the effect of the baffles, which decrease the tangential flow near the tank wall.

Although the velocity profiles appear to be flatter and have lower velocities at greater radial distances, the total flow increases. This indicates that entrainment exists in the turbine jet. Figure 19 shows the variation of flow rate with radial distance, and it is noted that the limiting value of flow measured at a radial distance of 5", is 15 cu.ft./min., which is 1.8 times the pumping capacity at the turbine periphery. By using a technique similar to that used by Aiba (12), Nagata et al. (19) integrated the flow profiles throughout the tank, and also found that the total recirculation rate was approximately 1.8 times the pumping capacity.

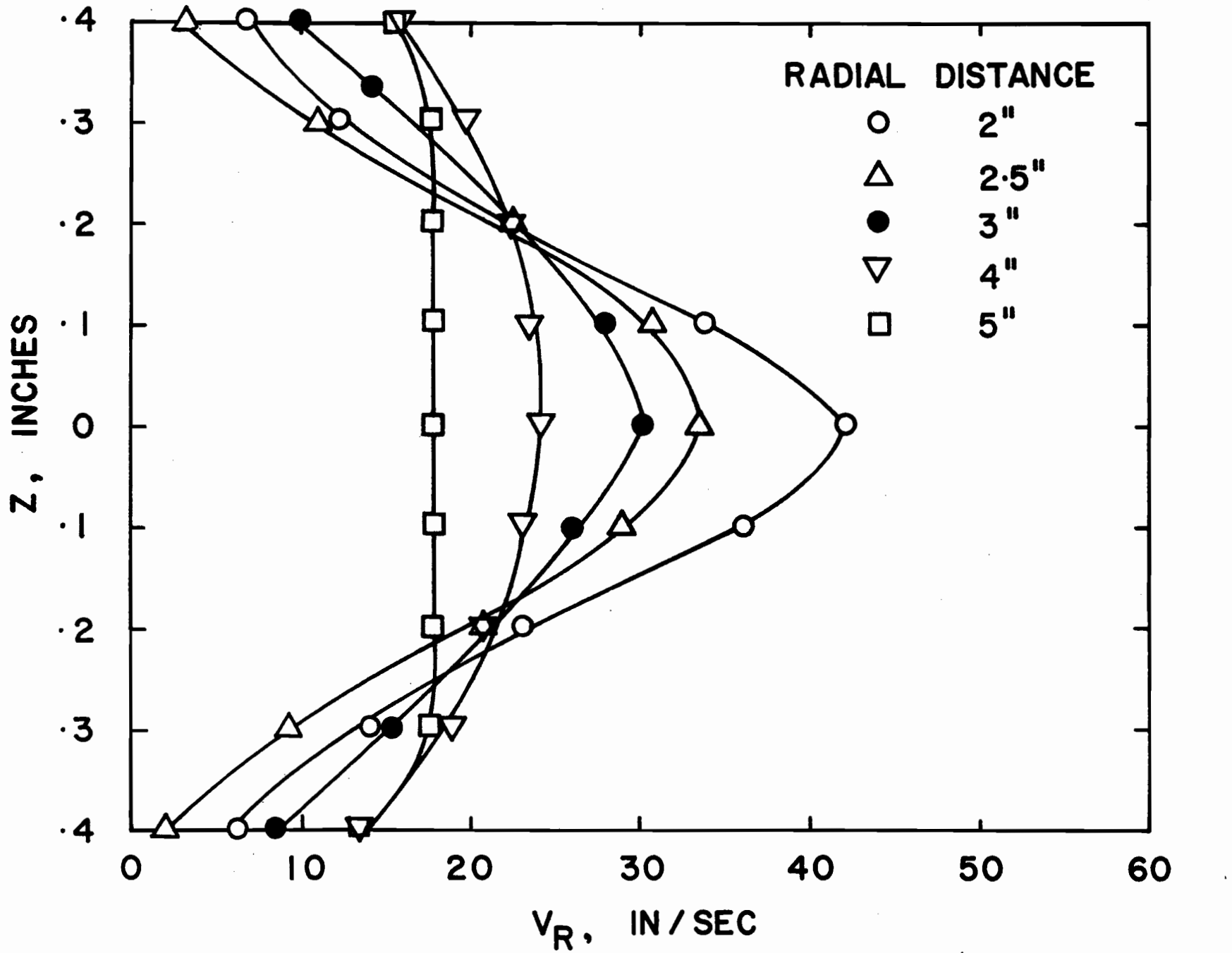

FIGURE 17 : RADIAL VELOCITY PROFILES AT DIFFERENT RADIAL DISTANCES (4" TURBINE IN WATER)

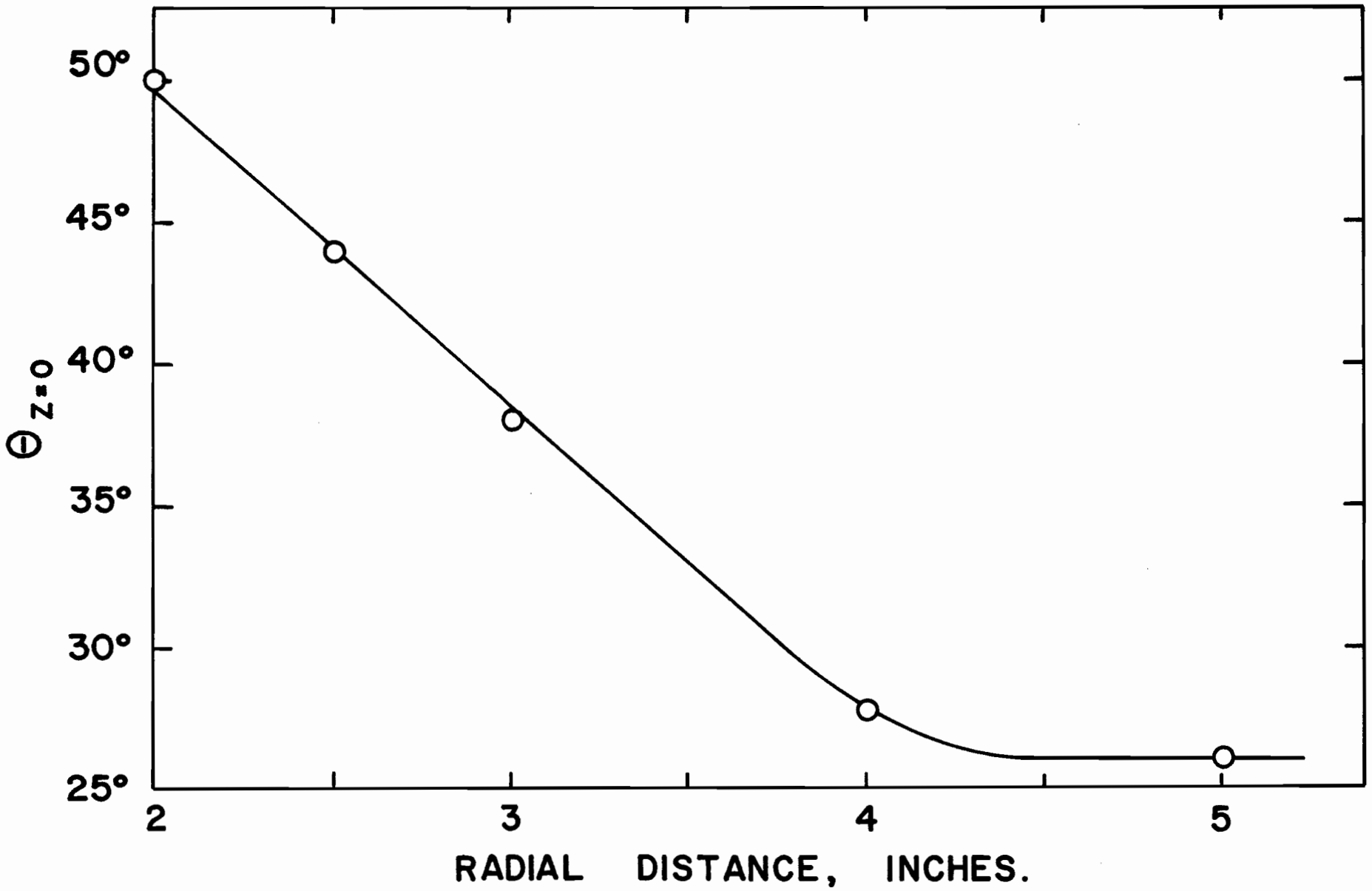

FIGURE 18 : VARIATION OF DIRECTION OF FLOW WITH RADIAL DISTANCE (4" TURBINE IN WATER)

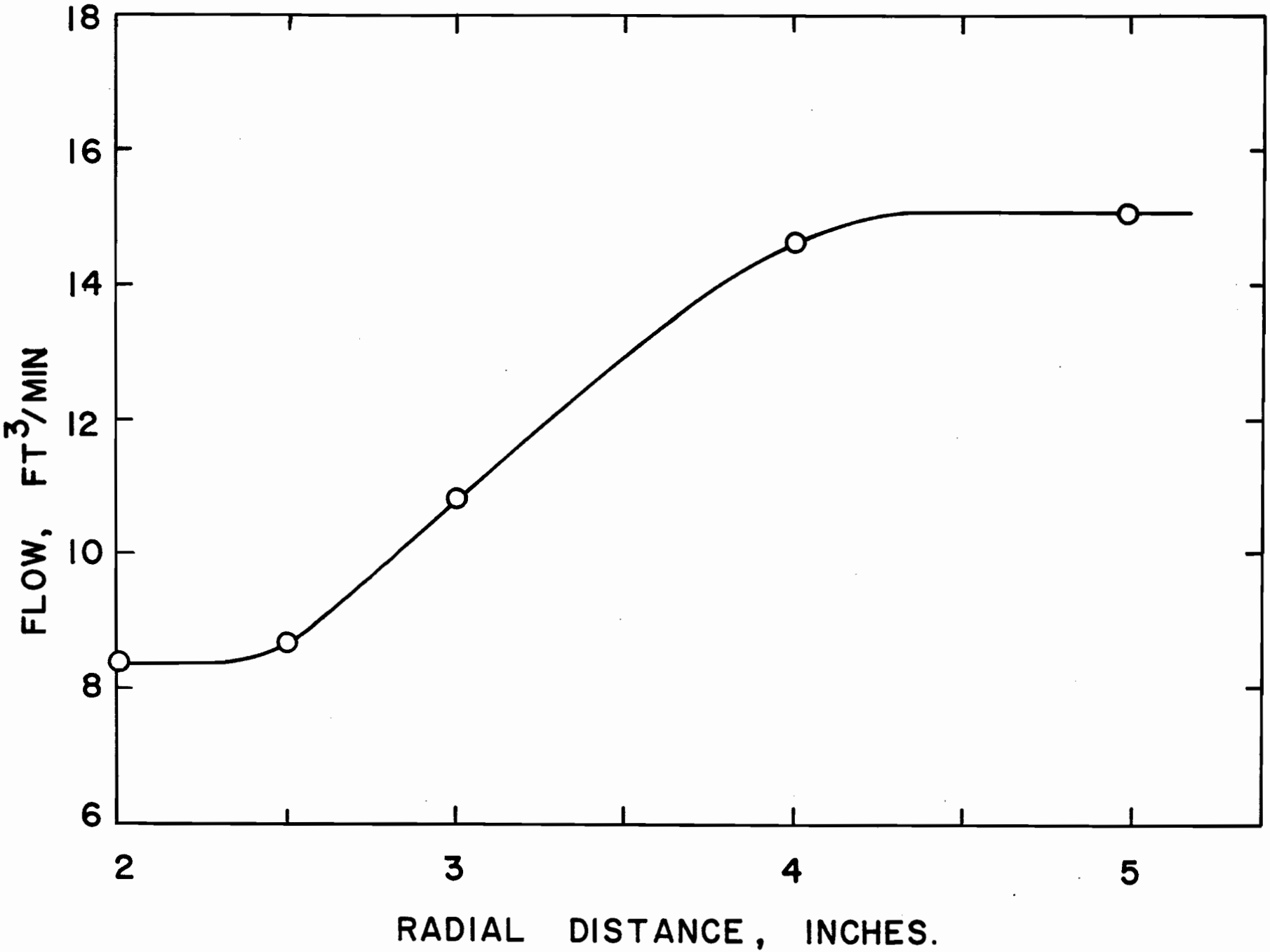

FIGURE 19 : VARIATION OF FLOW WITH RADIAL DISTANCE (4" TURBINE IN WATER)

Velocity and Angle Profiles Across Turbine Face

For the material balance between the pumping capacity in the discharge jet and the intake flow, the velocity profile across the face of the turbine was measured for several cases. Since the area of flow across the face of the turbine is considerably greater than the area round the circumference, the axial velocities in the intake were much lower than the discharge velocities. It is noted that the velocities are almost constant across the length of the blade, indicating a flat vertical profile in this region. Towards the centre of the turbine the velocities decrease to zero.

The hot wire was particularly useful in this case for obtaining velocity data, since it is particularly sensititve to lower velocities. The three dimensional pitot tube was necessary to determine the yaw and pitch angles. The velocity and angle data are tabulated in Appendix V.

Because of the lower velocities encountered, and also the fact that the flow is three dimensional, pumping capacities determined from the axial intake flow rather than the radial discharge, are likely to be less reliable, and this method was used only to serve as a check on the discharge results.

Turbine Pumping Capacities

When the radial velocity profile measured at the turbine periphery is integrated across the blade width and multiplied by the turbine circumference, the result is the pumping capacity.

From the theoretical development, an expression for the pumping capacity, Q is obtained, as given in Appendix II, and simplified to the form:

$$Q = K_{t_2} N D^3 \qquad (3)$$

where K_{t_2} is a coefficient depending on the W/D ratio. In most of the experimental work, the W/D ratio was 1/5.

Figures 20 and 21 demonstrate the linear relationship between the pumping capacity and the turbine rotational speed, while Figures 22 and 23 show the linear relationship of Q with the cube of the turbine diameter. The consistency of these experimental results with the theoretical development is evident. However, while K_{t_2} does not vary with rotational speed, it is slightly dependent on the turbine diameter. Values of K_{t_2}, evaluated for a number of cases with air and water, different sizes of turbines (W/D constant) and at various speeds, are tabulated in Table III. These values lie between 0.62 and 0.89. The theoretical development predicts values of K_{t_2} between 0.95 and 1.17.

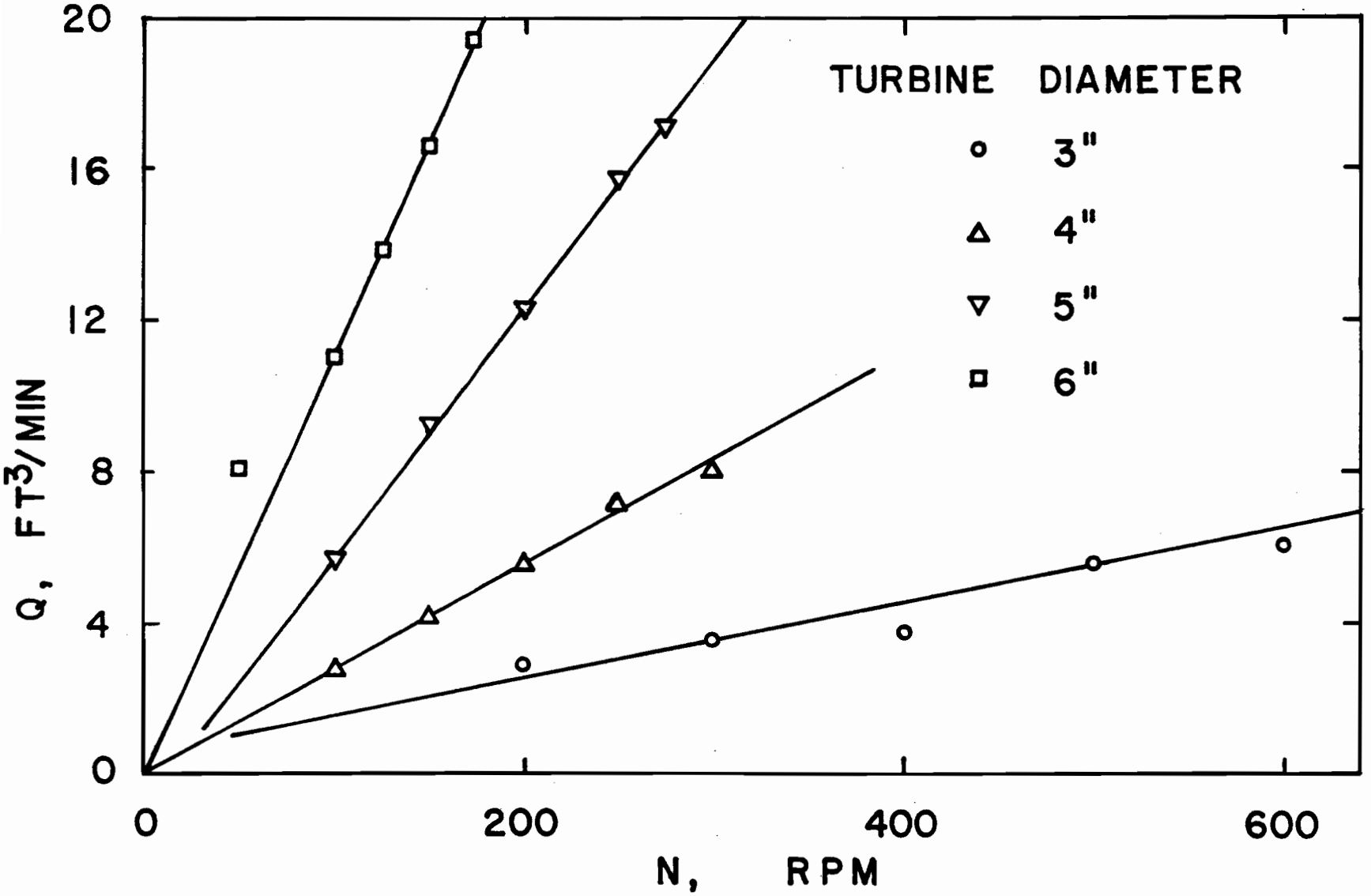

FIGURE 20 : VARIATION OF TURBINE PUMPING CAPACITY IN WATER WITH TURBINE SPEED

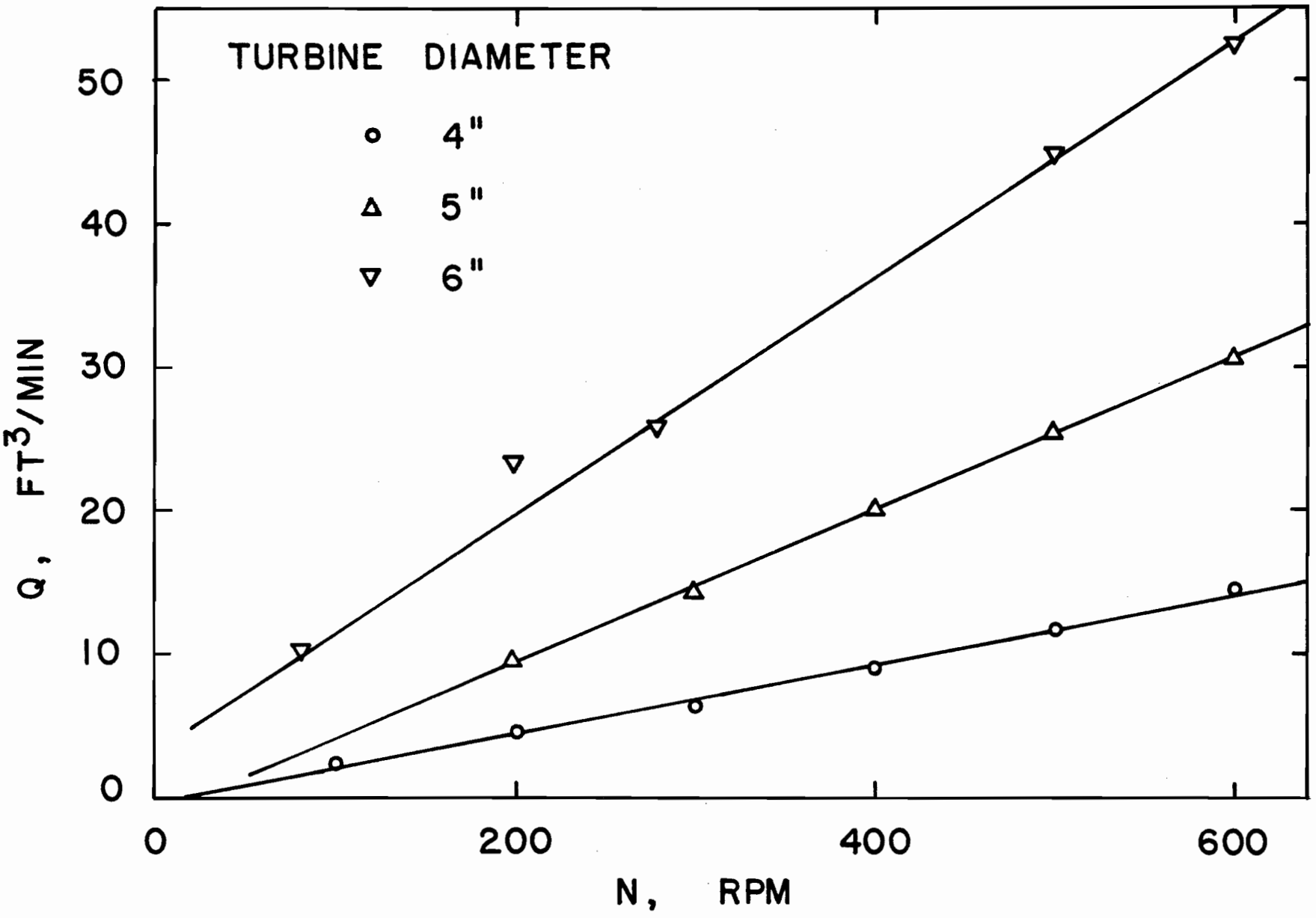

FIGURE 21 : VARIATION OF TURBINE PUMPING CAPACITY IN AIR WITH TURBINE SPEED

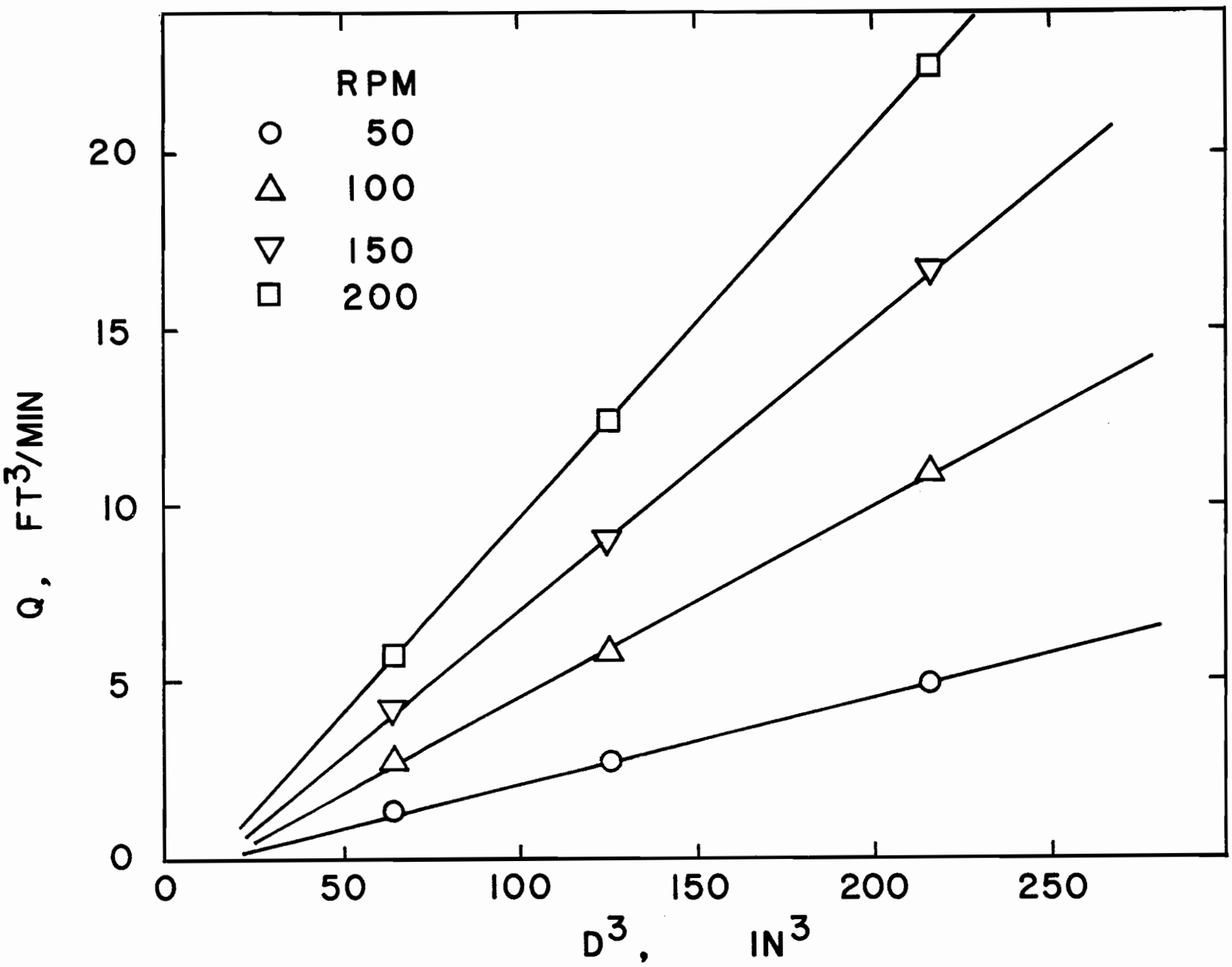

FIGURE 22 : VARIATION OF TURBINE PUMPING CAPACITY IN WATER WITH TURBINE DIAMETER

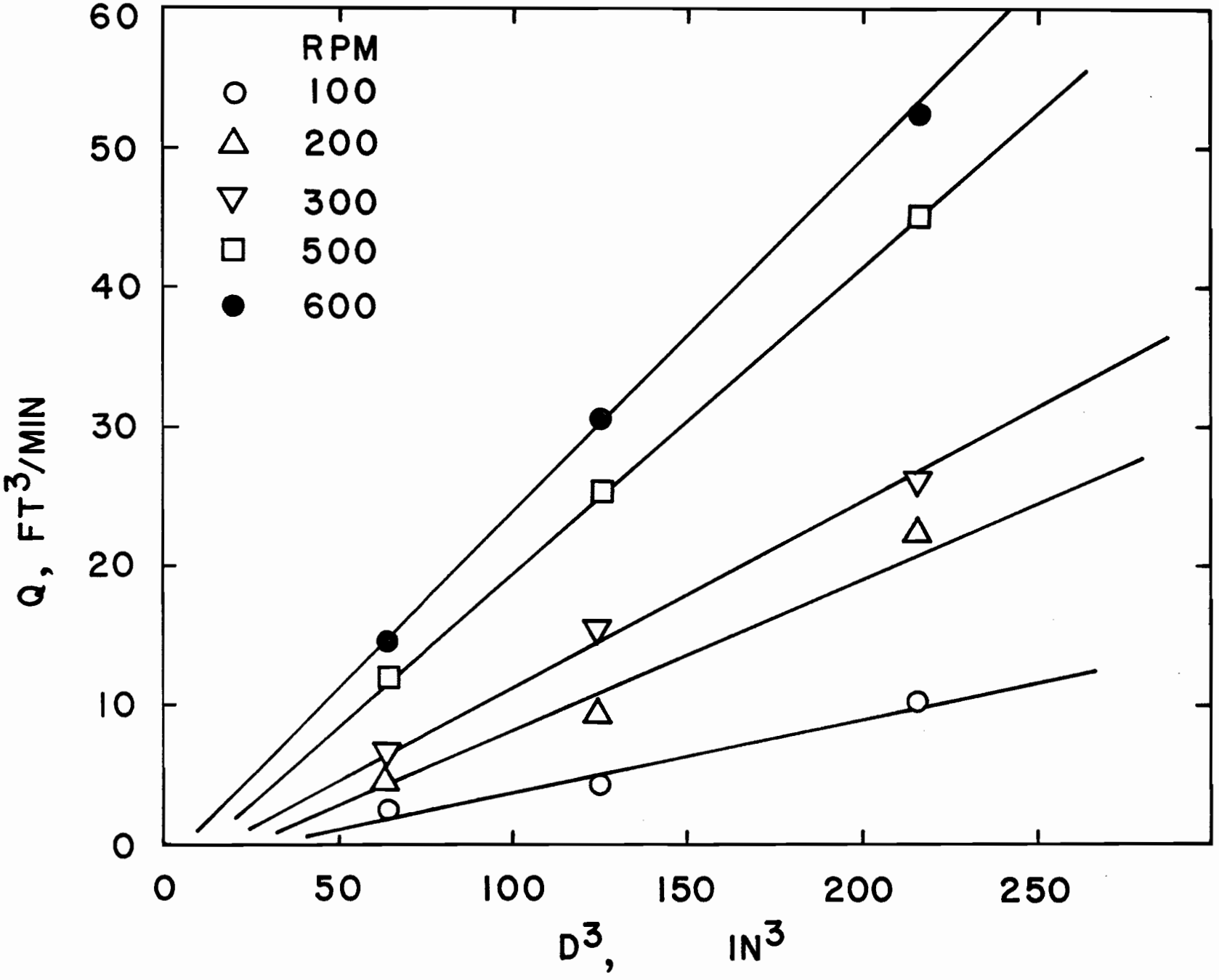

FIGURE 23 : VARIATION OF TURBINE PUMPING CAPACITY IN AIR WITH TURBINE DIAMETER

TABLE III

Experimental Values of K_{t_2} Averaged for Different Speeds

Turbine No.	Diameter in.	Water K_{t_2}	Water RPM Range	Air K_{t_2}	Air RPM Range
1	3	0.726	200-600	-	-
2	4	0.750	100-300	0.623	100-600
3	5	0.840	100-275	0.680	200-600
4	6	0.890	50-170	0.767	100-600

A comparison of these results with previously published work can be obtained from Table II. The values of K_{t_2} in Table II range from 0.47 to 1.4, indicating inconsistent results. Cutter (17) used the resultant velocity rather than the radial velocity to calculate the pumping capacity. Although the resultant velocity gives a measure of the fluid flow, the flow normal to the turbine periphery, i.e. the radial velocity, gives the volumetric through-put or pumping capacity. Holmes et al. (15) report a value of $K_{t_2} = 1.3$, very close to Cutter's, but have not indicated how they were able to obtain flow components using a propeller flowmeter, which implies that in effect, they also used the resultant velocity to calculate the pumping capacity.

Correcting the values of K_{t_2} obtained from the work of Cutter and Holmes et al. by evaluating the radial velocities using the angle of flow obtained from this work, it was found that K_{t_2} is in the range of 0.6 to 0.7 instead of 1.3 to 1.4. These corrected values are much closer to those reported by Sachs and Rushton (10) and Rushton et al. (9), and very close to the values obtained in this work.

Velocity Profile and Pumping Capacities with Varying Blade Width

Velocity measurements were made in water using a 4" turbine having six different sets of blades, ranging in width from 0.6" to 1.6". Two speeds, 100 and 200 RPM, were studied.

Figures 24 and 25 show the radial velocity profiles for the different blade widths at the two indicated speeds. Most noticeable is that regardless of the blade width, the radial velocities become zero at a finite distance along the blade width ($z \simeq 0.4$). The shapes of the curves and the magnitudes of the local velocities all depend on the width used. Both Figures 24 and 25 show that turbines having blade widths of 1.2-1.6" have similar radial velocity profiles, having a blunter shape and higher velocities. The three other blade widths, 0.6 to 1.0" can also be grouped together, since they exhibit the usual profiles, having a parabolic shape and lower velocities.

The angle profilesat the turbine periphery are shown in Figure 26 for the two speeds considered. Here again the results can be split into two groups:

(i) the larger blade widths, where the jet direction is more radial at the outer edges of the blade, and becomes more tangential towards the centre of the blade.

(ii) The usual case, where the blade widths are smaller, and velocity direction becomes increasingly radial towards the blade centre.

The 1.2" blade width shows the transition between the

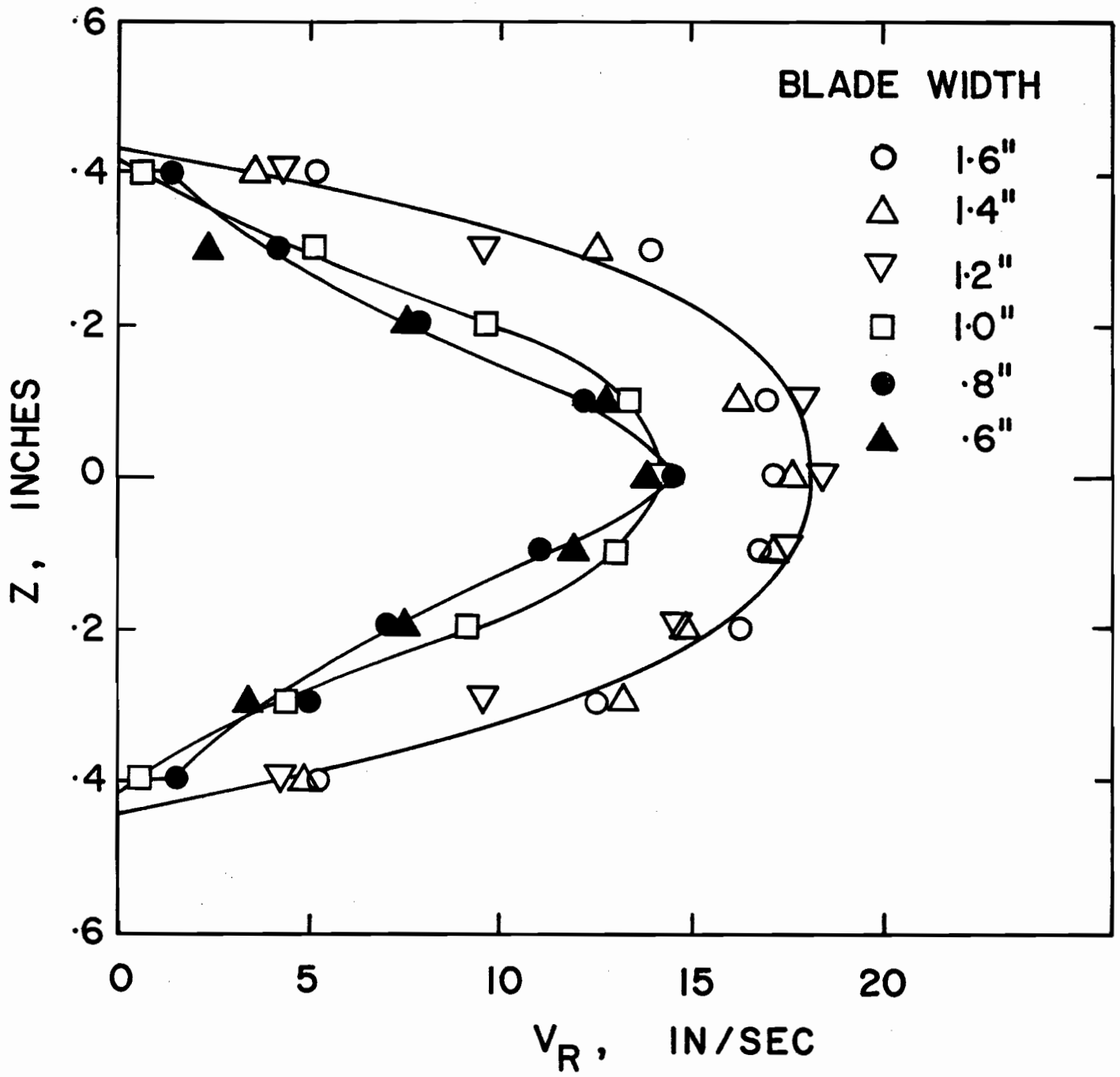

FIGURE 24 : EFFECT OF BLADE WIDTH ON RADIAL VELOCITY PROFILES (4" TURBINE IN WATER AT 100 RPM)

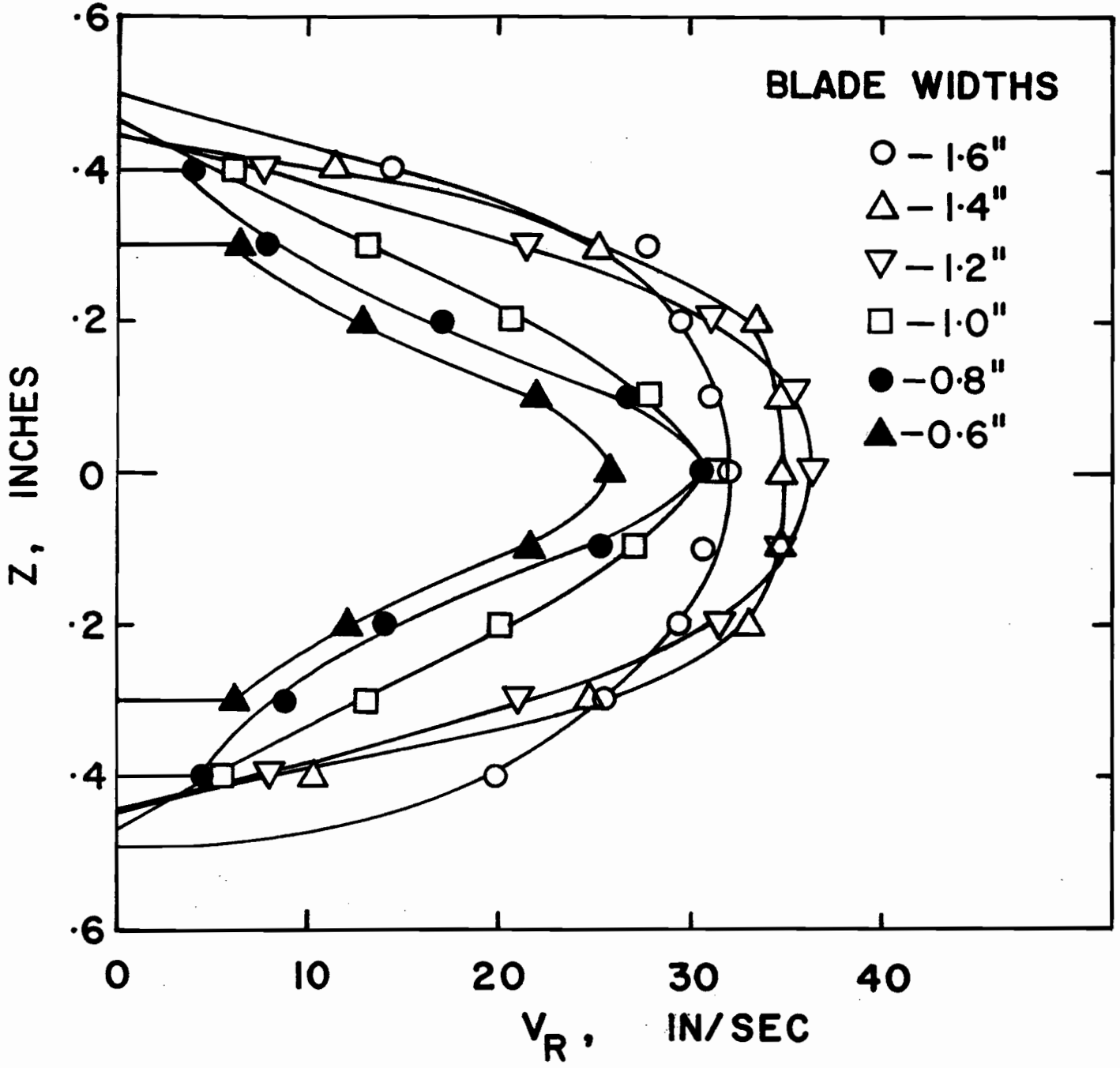

FIGURE 25 : EFFECT OF BLADE WIDTH ON RADIAL VELOCITY PROFILES (4" TURBINE IN WATER AT 200 RPM)

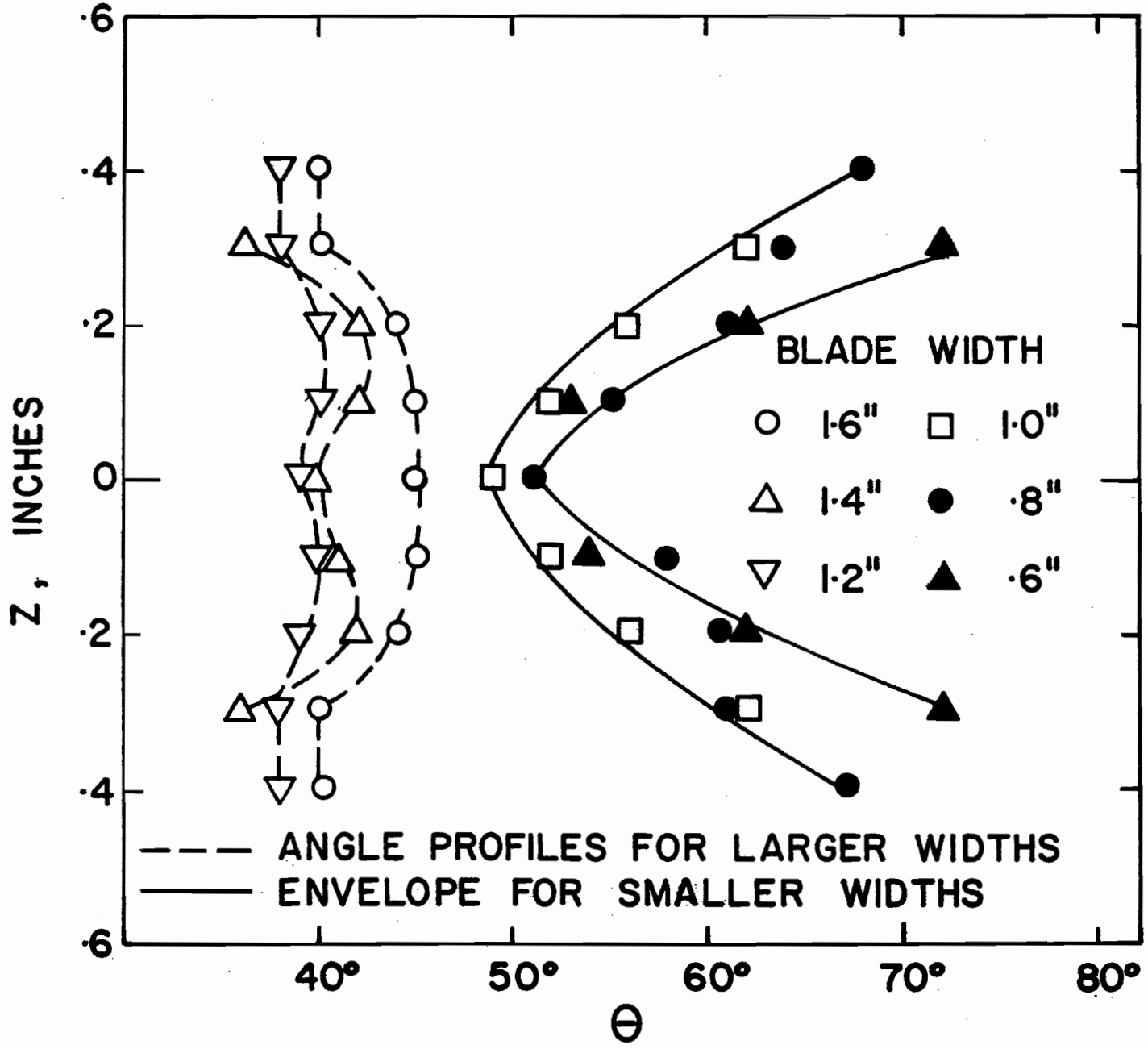

FIGURE 26 : EFFECT OF BLADE WIDTH ON ANGLE OF FLOW PROFILES (4" TURBINE IN WATER)

two cases.

Apparently some phenomena occurs with wider blades not previously detected. Holmes et al. (15) assumed that some average velocity or typical profile would exist across the entire width of the blade, regardless of the blade dimensions. However, the above experimental results show that this is evidently not the case. Moreover, this was checked with a 9" turbine in air, using smoke as a tracer to indicate the flow patterns. It was clearly visible that radial flow did not exist across the entire blade width for turbines of larger W/D ratios. It is interesting to note that the theoretical equation obtained (4) predicts that the radial velocity is zero at $z/R = 3\pi/16$, while the observed value is approximately $z/R = 1/5$.

From the radial velocity profiles the pumping capacities were calculated. Figure 27 shows the variation of Q with blade width for the two speeds. In the region where $W/D = 1/5$, the pumping capacity appears to vary almost linearly with the width, while at greater values of W, a limiting value of Q is reached.

This result is not surprising, if one considers the case of a turbine with an infinite blade width. To supply the discharge across the entire blade width, an infinite amount of intake flow would be required. Such a situation is unrealistic, and therefore one expects Q to reach a limiting value.

From this work, it appears that the ratio $W/D = 1/5$, is close to the value of the optimum blade width and any

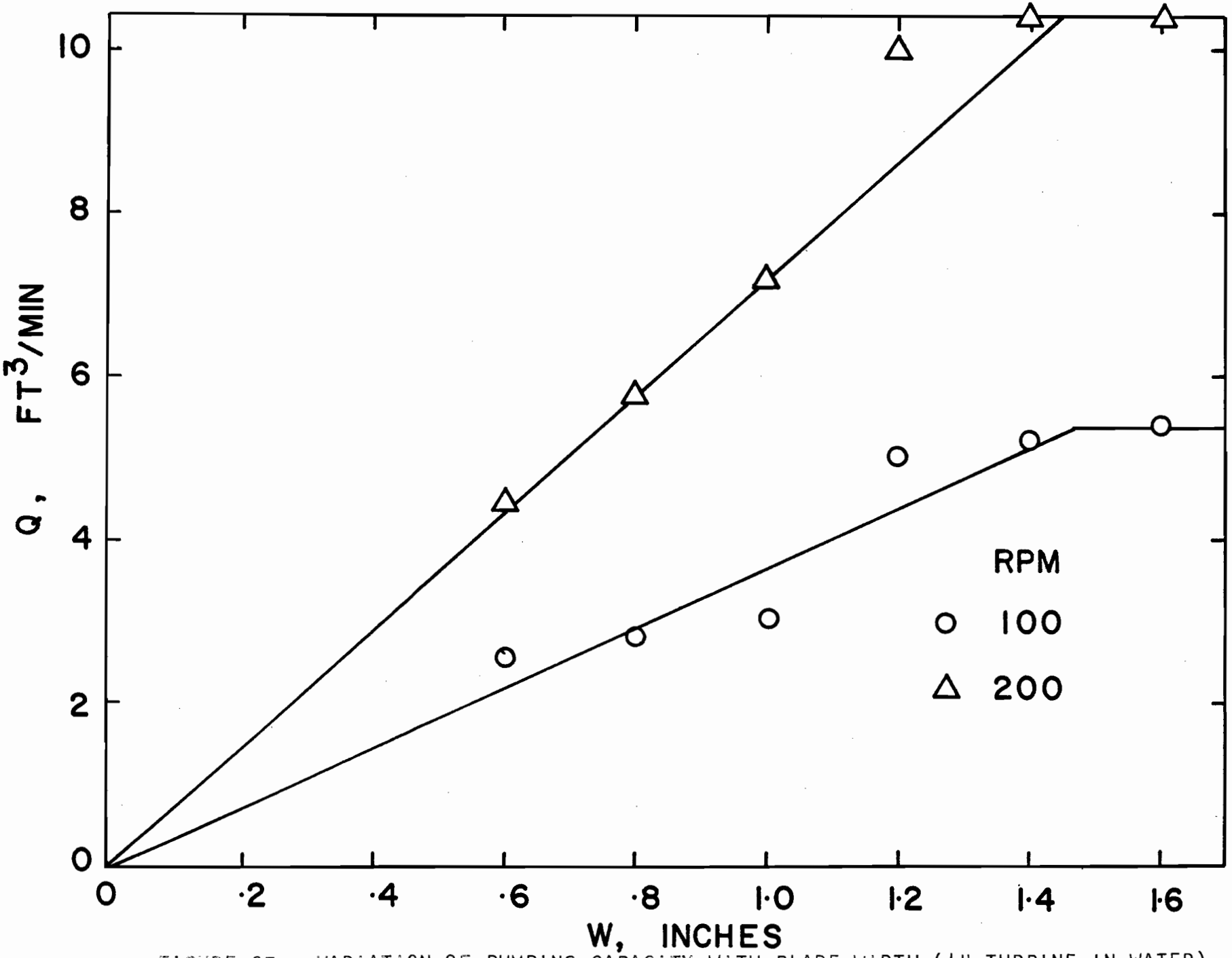

FIGURE 27 : VARIATION OF PUMPING CAPACITY WITH BLADE WIDTH (4" TURBINE IN WATER)

significant increase in width above this figure results in little change in the pumping capacity. It is interesting to note that this W/D ratio coincides with the standard turbine dimension generally used in the design of turbines.

Application of the Pumping Capacity

Since mixing in a tank takes place chiefly in the highly agitated region around the impeller, the pumping capacity should be a main factor in the degree of mixing achieved. Therefore, measurable quantities which depend upon the degree of mixing, such as the intensity of segregation, conversion in a stirred tank reactor etc., should be related to the pumping capacity. Most experimental data available for mixing systems have been correlated against the Reynold's Number, impeller speed, turbine diameter and others, rather than the pumping capacity, which is a more direct measure of mixing. This is primarily a result of the lack of knowledge concerning pumping capacities, particularly in the case of turbine impellers. Having obtained a suitable method for determining pumping capacities of turbines, which can be extended to other types of impellers, correlations of mixing data against this value became possible. The use of the pumping capacity was also extended to evaluate the Power Number.

The intensity of segregation is a mixing tank parameter defined to give the "goodness of mixing" in a stirred vessel, and has been measured by several researcher. The intensity of segregation was defined by Danckwerts (20) as:

$$I = \frac{\sigma_a^2}{\bar{a}\,(1 - \bar{a})} \tag{7}$$

where $\sigma_a^2 = \lim_{T\to\infty} \frac{1}{T} \int_0^T (a - \bar{a})^2 \, dt$

= the variance in concentration of A at a point

$\bar{a}$ = average concentration of A

a concentration of A at the point

The intensity of segregation describes the goodness of mixing by measuring the interdiffusion of concentration clumps using the concept of concentration at a point.

Using the pumping capacity and the age distribution of the particles in the tank, in the theoretical development given in Appendix IV, the following equation for the intensity of segregation was obtained for a continuous stirred tank operation:

$$I = \frac{F}{Q + F} \tag{8}$$

It is noted that as Q becomes infinite (perfect mixing), the intensity of segregation becomes zero, while as Q approaches zero (no impeller mixing), the intensity goes to unity.

This relationship was compared to the data available in the literature. Kang (21) has measured the intensity of segregation in a stirred tank, and has studied the effect of various parameters such as feed rate and impeller speed. He obtained a variety of curves relating the intensity of segregation in the

outlet stream to the impeller speed for different feed rates, but did not report any general correlation. Figure 28, using Kang's data, shows that a general curve can be obtained by plotting F/(Q + F) against the intensity of segregation. With the limited data available, a similar curve has been drawn using the results of the work of Manning and Wilhelm (22). The ratio of the square root of the concentration variance to the mean concentration is plotted against F/(Q + F). Here different sizes of turbines were used, and again a single curve correlates the results, as shown in Figure 29.

In both cases the intensity of segregation, while showing a definite relationship with F/(Q + F), did not equal this ratio. This can be explained by noting that neither Kang nor Manning and Wilhelm measured the concentration variance at a point, but considered the variance for a finite volume. This does not, however, lessen the importance of using the ratio of F/(Q + F) as a convenient group to correlate intensity of segregation and concentration variance data. It indicates also the importance of measuring the concentration fluctuations for infinitely small volumes.

In other work, Worrell and Eagleton (23) measured the conversion for a second order reaction in a continuous stirred tank reactor as a function of speed and residence time. Using this data, Manning, Wolf and Keairns (6) were successful in correlating a dimensionless concentration against the Q/F ratio. The pumping capacity, which determined the degree of mixing in

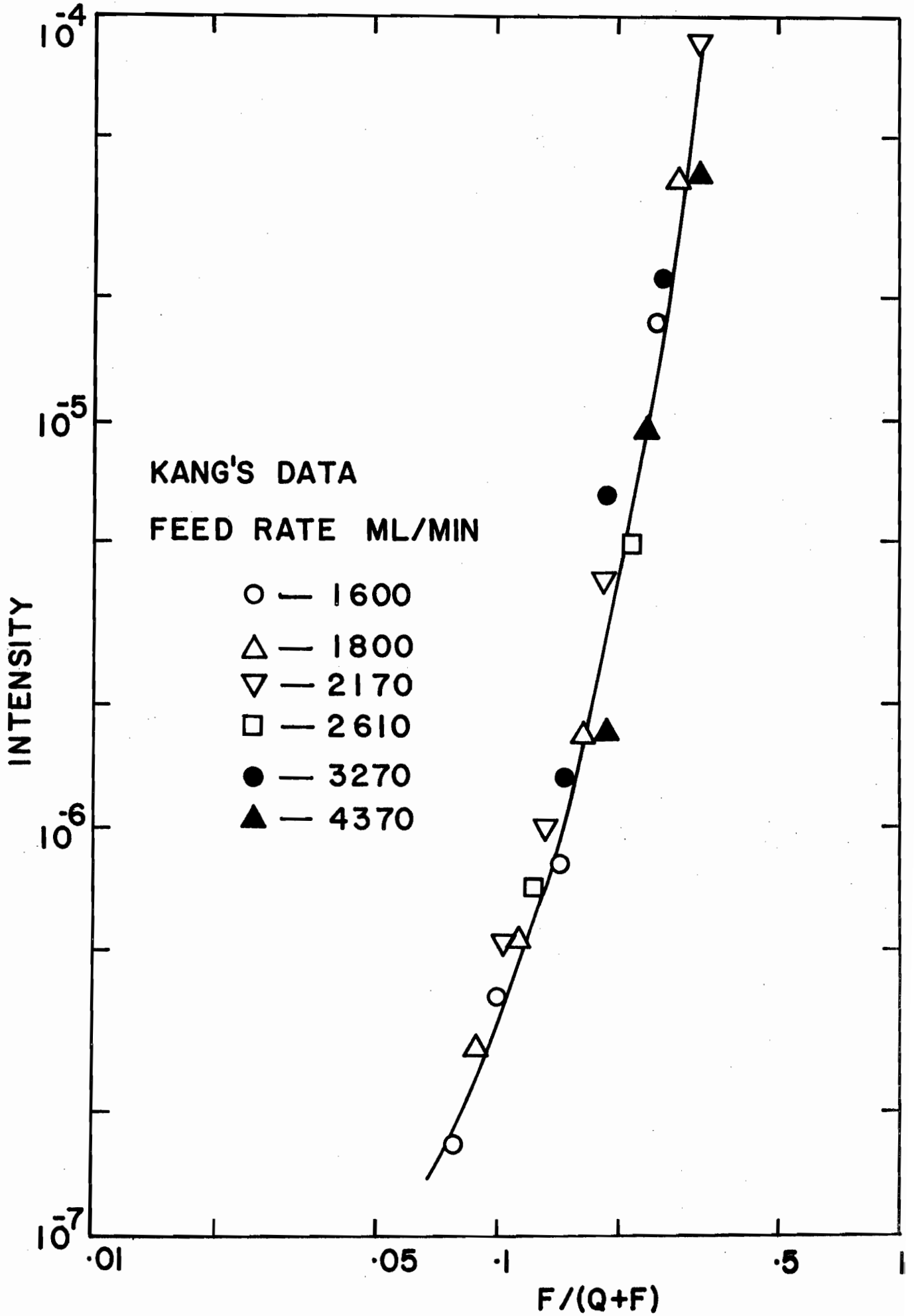

FIGURE 28 : EFFECT OF TURBINE PUMPING CAPACITY ON INTENSITY OF SEGREGATION

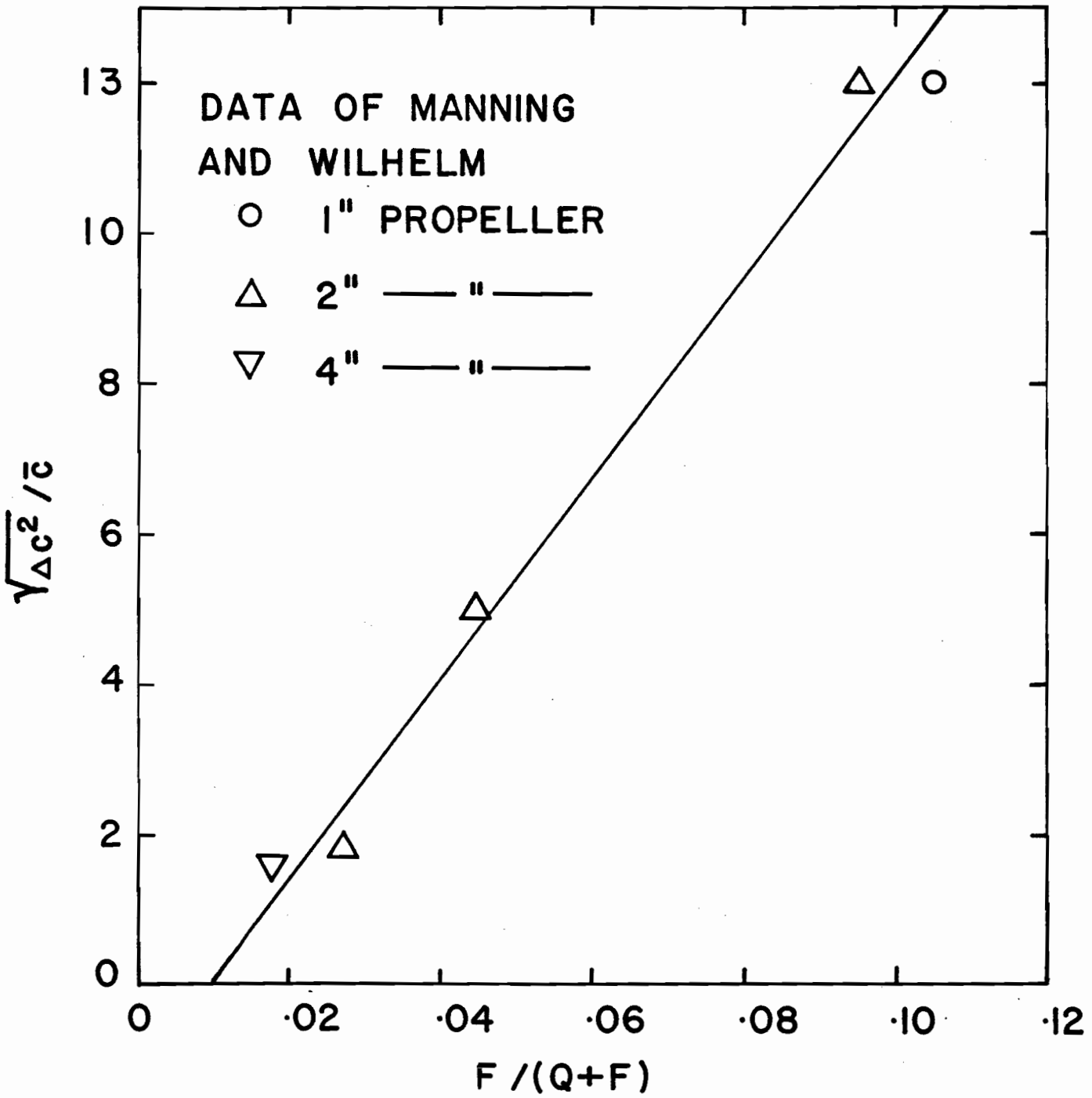

FIGURE 29 : VARIATION OF CONCENTRATION VARIANCE WITH PROPELLER PUMPING CAPACITY

the vessel, was a convenient measure of the conversion deviation from the ideal mixing case.

The pumping capacity is also useful to determine the form of the Power Number for an impeller. The power requirement is the product of the mass flow rate and the head developed by the impeller. For a turbine,

$$\text{Power} = \text{head} \times \text{mass flow}$$

$$= \text{head} \times \text{pumping capacity} \times \text{density}$$

$$P = \frac{\pi^2 D^2 N^2}{2g} \cdot 0.75\, ND^3 \rho \qquad (9)$$

$$\text{or} \quad \frac{Pg}{\rho N^3 D^5} = \frac{\pi^2 \times 0.75}{2} = 3.6$$

Grouping the variables together in the term on the left, results in a dimensionless group, and is in fact, the Power Number. The value of the Power Number evaluated by this method is 3.6 compared to 6.3 reported by Rushton et al. (3) for a 6-blade turbine for higher Reynolds Numbers.

A similar development for the case of propellers also gives the dimensionless Power Number when the variables are grouped together. Here the velocity in the head term was taken as $4Q/\pi D^2$, where head = $v^2/2g$. A value of $N_{Po} = 0.10$ is obtained compared to the value reported by Rushton et al. of 0.32 for a 3-blade square pitched propeller.

CONCLUSIONS

The two dimensional pitot tube and the hot wire probe were used to determine the velocity profiles of turbine type impellers, and in turn, to evaluate the pumping capacities. Propellers were also checked for comparison. Both methods gave a similar result and showed:

1. The normalized radial velocity profiles of the turbine jet are independent of turbine speed and independent of turbine diameter for geometrically similar turbines.
2. The radial velocity profile is parabolic in shape, while the tangential profile is flatter.
3. An angle profile exists across the width of the blade. The flow becomes increasingly radial towards the centre-line of the turbine, for turbines of standard dimensions. The angle profile is independent of speed and turbine size for geometrically similar turbines.
4. The radial velocity profile becomes increasingly plug in shape with greater radial distances. The flow becomes more radial in direction, and the total flow increases due to the entrainment effect. The maximum jet flow, representing the recirculation rate, is 1.8 times the pumping capacity for the 4" turbine, and the system investigated.
5. The pumping capacity of a turbine can be correlated by the expression:

$Q = K_{t_2} ND^3$ for constant W/D or by:

$Q = K_{t_1} ND^2 W$ for W/D in the range of 1/5

6. The discharge coefficient, K_{t_2} was found to be independent of turbine speed, but varied with the turbine diameter and the fluid used. K_{t_2} for water was found to vary from 0.726 to 0.89 for turbine diameters ranging between 3" and 6", while for air, K_{t_2} ranged between 0.623 and 0.767 for diameters of 4" to 6".

7. The blade width of the turbine can be increased to a limit after which the radial velocities become zero. However the centreline velocity and the pumping capacity both increase with blade width, but tend to reach a limiting value.

8. The flow profiles across the turbine diameter are axial in nature with yaw angles between 0^o and 10^o, and pitch angles between 0^o and 30^o. The velocity profile is almost flat along the blade length and decreases as the centre is approached. The intake velocities are much lower than the discharge velocities.

9. The comparison of flows entering the turbine across the diameter, and leaving across the blade width were found to be within 6% accuracy for the pitot tube, and 2% for the hot wire probe, which proved the validity of the two methods.

10. Using a propeller, the pumping capacities and velocity profiles as determined by both experimental methods, gave results consistent with the work of other researchers ($K_p = 0.53$), which again proved the validity of the methods.

11. The use of smoke as a tracer in determining velocity profiles and flow patterns, qualitatively verified some of the above conclusions.

12. The pumping capacity was found to be a convenient term to correlate intensity of segregation, conversion in a continuous stirred tank reactor and the Power Number.

NOMENCLATURE

a - concentration of A at a point

a - concentration of A in feed stream

$\bar{a}$ - average concentration of A in tank

A - component "A" in system

b - variable used in Appendix II

c - concentration

C_1 - parameter defined in Appendix II

D - turbine diameter

$E(t)$ - distribution function

f - function

F - volumetric feed rate to tank

g - acceleration due to gravity

i - $\sqrt{-1}$

I - intensity of segregation

$I(t)$ - age distribution function

k - parameter defined in Appendix II

K_p - propeller discharge coefficient

K_{t_1} - turbine discharge coefficient defined in equation (3)

K_{t_2} - turbine discharge coefficient defined in equation (3)

L - turbine blade length

n - number of propeller blades

N - impeller rotational speed (R.P.M.)

N_{Fr} - Froude Number = $\frac{ND^2}{g}$

N_{Po} - Power Number = $\frac{Pg}{\rho N^3 D^5}$

N_{Re} - Impeller Reynolds Number = $\frac{\rho N D^2}{\mu}$

P - power

P_1 - total pressure tap - 2 and 3 dimensional pitot tubes

P_2, P_3 - static pressure taps - 2 and 3 dimensional pitot tubes

P_4, P_5 - pitch angle pressure taps - 3 dimensional pitot tube

Q - pumping capacity

r - radial co-ordinate in cylindrical co-ordinate system

R - impeller radius

t, T - time

v - velocity

v_a - inlet flow rate of component A

v_o - inlet flow of second stream

V - volume

V_r - radial velocity component at r

V_R - radial velocity component at turbine radius R

V_Z - vertical velocity component at z

W - turbine blade width

X - radial distance (Appendix III)

z - vertical co-ordinate in cylindrical co-ordinate system

α - variable used in Appendix II

β - variable used in Appendix II

β - angle of flow at radial distance X

μ - viscosity

θ - angle of flow in turbine discharge jet

θ - pitch angle of propeller (Appendix I)

θ, θ' - mean residence times (Appendix IV)

ρ - density

σ - variance

ω - angular velocity

BIBLIOGRAPHY

1. White, A. M. and Brenner, E., Trans. A.I.Ch.E., 30, 585 (1934).

2. Hixson, A. W. and Baum, S. J., I.E.C., 34, 194 (1942).

3. Rushton, J. H., Costich, E. W. and Everett, H. J., C.E.P., 46, 395 (1950).

4. Van de Vusse, J. G., C.E.Sci., 4, 178 (1955).

5. Norwood, K. W. and Metzner, A. B., A.I.Ch.E.J., 6, 432 (1960).

6. Manning, F. S., Wolf, D. and Keairns, D. L., "Model Simulation of Stirred Tank Reactors" (unpublished), Carnegie Inst. Tech.

7. Danckwerts, P. V., Chem. React. Engrg., 1, 93 (1957).

8. Cholette, A., paper presented Chem. Inst. Can., Quebec, Nov. 1965.

9. Rushton, J. H., Mack, D. E. and Everett, H. J., Trans. A.I.Ch.E., 42, 441 (1946).

10. Sachs, J. P. and Rushton, J. H., C.E.P., 50, 597 (1954).

11. Metzner, A. B. and Taylor, J. S., A.I.Ch.E.J., 6, 109 (1960).

12. Aiba, S., ibid., 4, 485 (1958).

13. Porcelli, J. V., Jr., and Marr, G. R., Jr., I.E.C. Fundamentals, 1, 172 (1962).

14. Marr, G. R. Jr., and Johnson, E. F., A.I.Ch.E.J., 9, 383 (1963).

15. Holmes, D. B., Voncken, R. M. and Dekker, J. A., C.E.Sci., 19, 201 (1964).

16. Wolf, D. and Manning, F. S. (to be published), Can.J. of C.E., June 1966.

17. Cutter, L. A., A.I.Ch.E.J., 12, 35 (1966).

18. Neilson, J. H., Ph.D. Thesis, I.I.T. (1958).

19. Nagata, S., Yamamoto, K., Hashimoto, K. and Naruse, Y., Mem. Fac. Engrg., Kyoto, 21, 260 (1959).

Leaf following 68 omitted in numbering.

20. Danckwerts, P. V., App. Sci. Research 3, (1953).

21. Kang, W. K., Ph.D. Thesis, U. of Minn. (1960).

22. Manning, F. S. and Wilhelm, R. H. Wilhelm, A.I.Ch.E.J., 9, 12 (1963).

APPENDIX I

Pumping Capacity of a Propeller

A propeller with n blades and a pitch angle of θ is considered. Figure 30a shows a simplified sketch of the projected area of one of the blades of the propeller. For simplicity the projected area is taken to be a segment of a circle with arc length $2\pi R/n$ at the circumference, and arc length $2\pi r/n$ at any radius r. The annular section of radius r and width Δr is considered in Figure 30b. The height of the section is $2\pi r \tan\theta /n$.

If the blade makes $\frac{1}{n}$ revolutions, a certain volume of fluid is displaced in a downward direction. This volume equals the product of the height and the projected area of the element.

$$\text{Volume displaced for } \frac{1}{n} \text{ revolutions} = \frac{2\pi r \tan\theta}{n} \cdot \frac{2\pi r.dr}{n}$$

If the blade rotates at a speed N revolutions per unit time, then the volume displaced is:

$$\text{Volume/unit time} = \frac{2\pi r \tan\theta}{n} \cdot \frac{2\pi r.dr}{n} \cdot n \times N$$

Considering the summation of the differential sections comprising the blade for $0 \leq r \leq R$, the volume displaced per unit time is:

$$\text{Volume/time} = \int_0^R \frac{4\pi^2 N}{n} \tan\theta \, .r^2.dr$$

and the total displaced or pumping capacity for n blades is

$$Q = \frac{\pi^2 N \tan\theta . D^3}{6} \qquad \text{(A-1)}$$

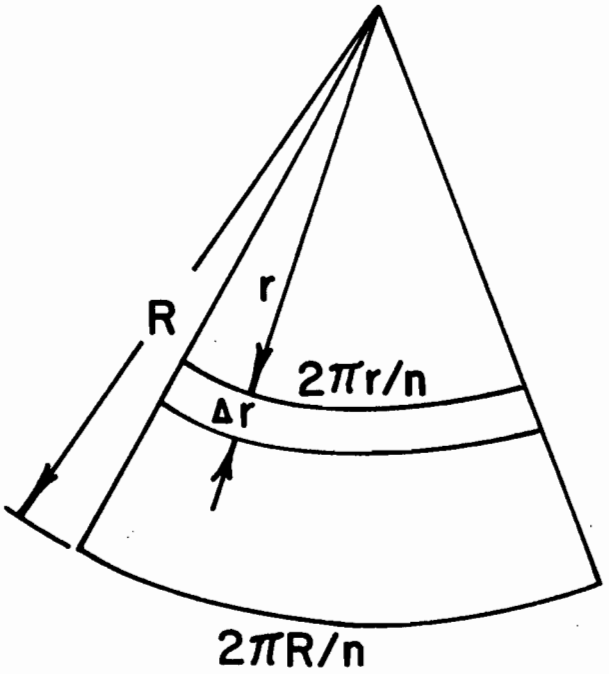

FIGURE 30a

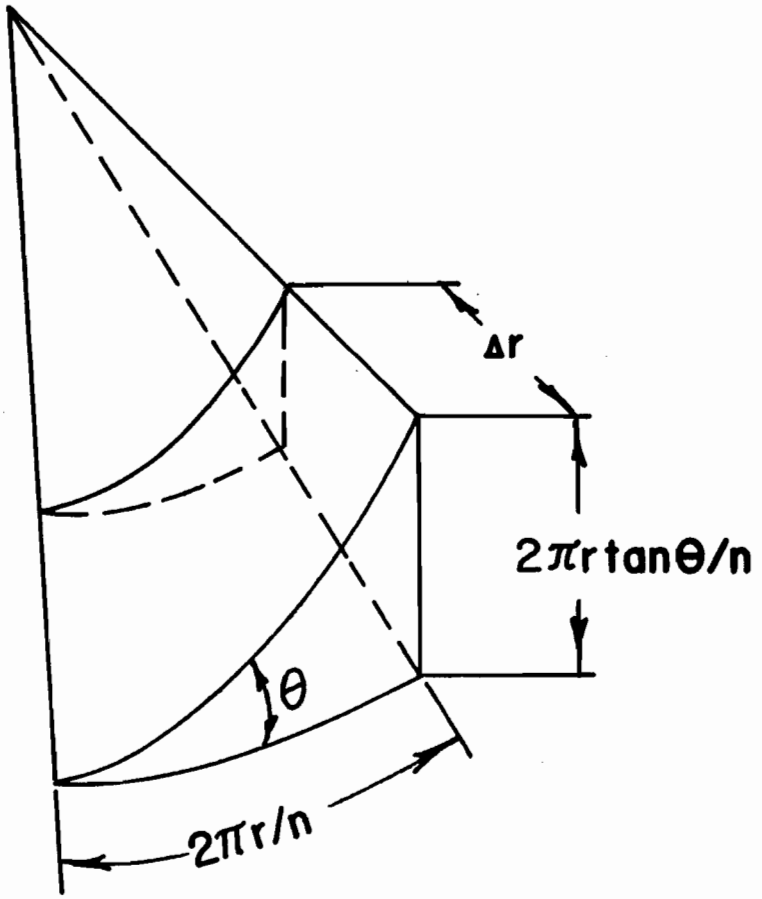

FIGURE 30b

FIGURE 30a : SKETCH OF PROJECTED AREA OF PROPELLER AREA

FIGURE 30b : ELEMENT OF PROPELLER BLADE

For a pitch of 45^{o}, the expression becomes:

$$Q = \frac{\pi^2 ND^3}{6} = 1.65\ ND^3 \qquad (A\text{-}2)$$

For a pitch of 30^{o}, the expression for Q becomes:

$$Q = 0.95\ ND^3 \qquad (A\text{-}3)$$

Thus the pumping capacity of a propeller can be written in the form:

$$Q = K_p ND^3$$

Since the frictional forces, the curved shape of the propeller and the changing pitch angle have all been neglected, it is expected that experimental values of K_p will be somewhat lower than those obtained from Equation(A-1).

APPENDIX II

Expressions for Velocity Profiles and Pumping Capacities of Turbines

It was desired to obtain a simple relationship to describe the velocity profiles and pumping capacities of a turbine in terms of the geometry and speed of the system. Considering the equations of motion and continuity in three dimensions does not give a simple solution. The following development, although over-simplified, gives the desired relationship.

Consider the cross-hatched section as shown in Figure 31. This region represents an annular section of the fluid in the turbine, having outer radius R and inner radius kR, and width Δz. The fluid in the physical confines of the turbine is assumed to behave like a solid core rotating at the angular velocity of the turbine, ω, with a small inner stagnant core of radius kR. Since for most turbines, the length of the blade is half the radius, the limit for k will be:

$$0 \leq k \leq 1/2$$

It is further assumed that V_z, the vertical velocity has a flat profile for $kR \leq r \leq R$, and is zero for $r \leq kR$. This means that $V_r = 0$ at $r \leq kR$.

If the equation of motion in the radial direction is considered in differential form, the term $\rho V_\theta{}^2/r$ represents the changes in momentum in the rotating system effected by the

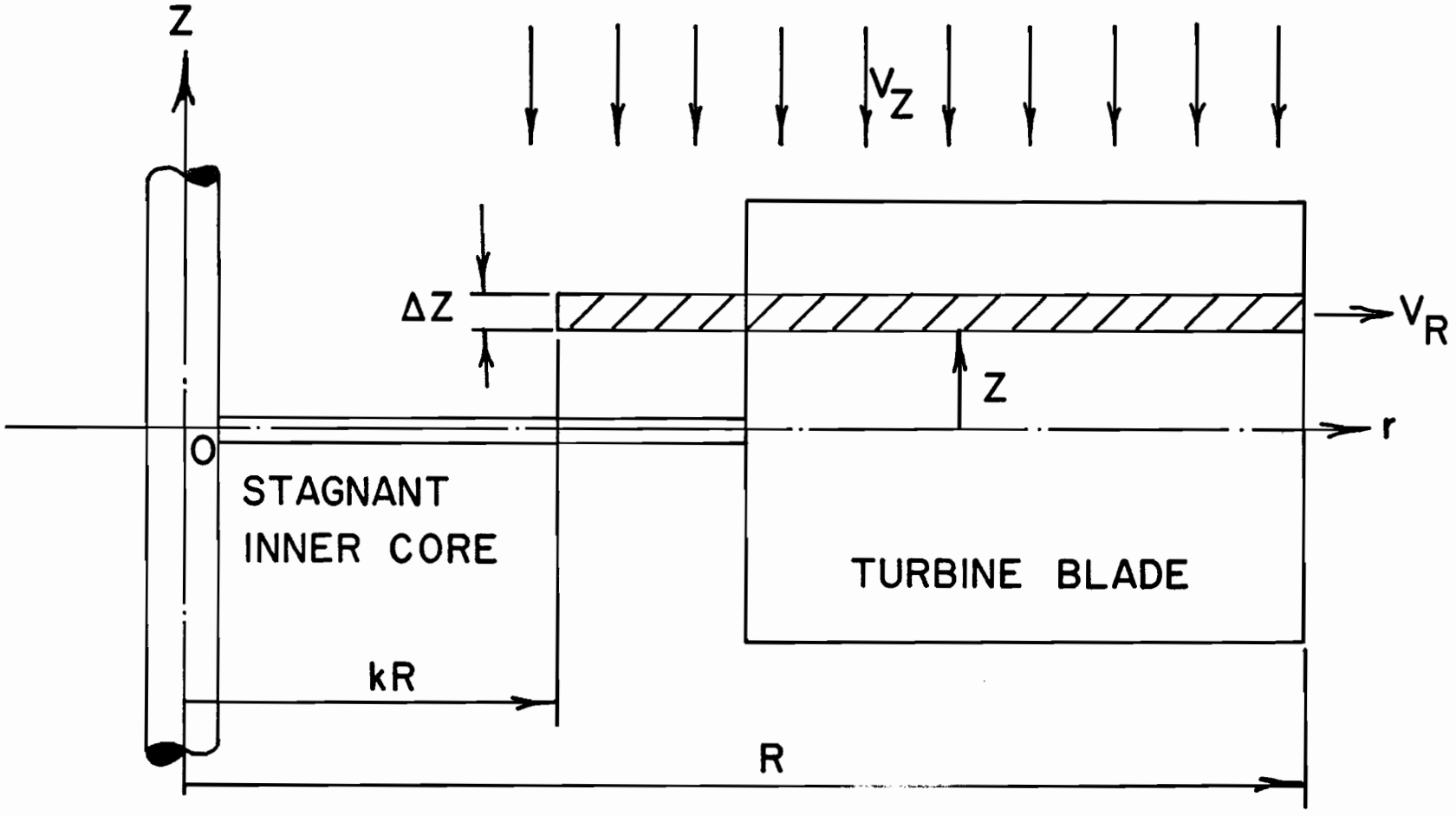

FIGURE 31 : ANNULAR SECTION OF TURBINE

rotating fluid. ($V_\theta = \omega r$ = angular velocity).

Considering this term from kR to R:

$$\text{the centrifugal force} = \int_{kR}^{R} \rho V_\theta{}^2/r.dr$$

$$= \int_{kR}^{R} \rho \omega^2 r.dr. = \frac{\rho \omega^2 R^2}{2}(1 - k^2)$$

and for the annular element, by multiplying by $2\pi R \Delta z$, is:

$$\text{the centrifugal force} = \rho \pi \omega^2 R^3 (1-k^2) \Delta z \qquad (A-4)$$

A material balance over the annular element gives:

$$-\rho V_z \pi (R^2-k^2R^2)\Big|_{z+\Delta z} + \rho V_z \pi (R^2-k^2R^2)\Big|_z - 2\pi R \Delta z \rho V_R = 0 \qquad (A-5)$$

Neglecting viscous forces, a momentum balance gives:

$$-\rho V_z{}^2 \pi (R^2-k^2R^2)\Big|_z + \rho V_z{}^2 \pi (R^2-k^2R^2)\Big|_{z+\Delta z} + 2\rho \pi R V_R{}^2 \Delta z = \rho \pi^2 \omega^2 R^3 (1-k^2) \Delta z \qquad (A-6)$$

In differential form, equation (A-5) for the material balance becomes:

$$\frac{dV_z}{dz} = \frac{-2V_R}{(1-k^2)R} \qquad (A-7)$$

and equation (A-6) becomes:

$$(1-k^2)R \frac{d(V_z{}^2)}{dz} = -2V_R{}^2 + (1-k^2)\omega^2 R^2 \qquad (A-8)$$

Substituting the value of dV_z/dz from (A-7) into (A-8) gives:

$$V_R = V_z + \sqrt{V_z^2 + \tfrac{1}{2}(1-k^2)\,\omega^2 R^2} \qquad \text{(A-9)}$$

Substituting the value of V_R from (A-9) into (A-7), equation (A-10) is obtained:

$$\frac{dV_z}{V_z + \sqrt{V_z^2 + C_1^2 \omega^2 R^2}} = \frac{dz}{C_1^2 R} \quad \text{where } C_1 = \sqrt{\tfrac{1}{2}(1-k^2)} \qquad \text{(A-10)}$$

Integrating (A-10) gives:

$$\int_0^{V_z} \frac{dV_2}{V_z + \sqrt{V_z^2 + C_1^2 \omega^2 R^2}} = \frac{z}{C_1^2 R} \qquad \text{(A-11)}$$

The integral on the left is of the form:

$$\text{Integral} = \int_0^x \frac{dx}{x + (x^2+b^2)^{\frac{1}{2}}} \quad \text{where } x = V_z$$

$$b = C_1 \omega R \qquad \text{(A-12)}$$

and noting that $x/b < 1$, (A-12) can be written as:

$$\text{Integral} \int_0^x \frac{2b.dx}{x^2+2bx+2b^2} \qquad \text{(A-13)}$$

The integral can be solved by finding the complex roots of the denominator:

$$\text{Integral} \int_0^x \frac{-i\,dx}{x+b-ib} + \int_0^x \frac{i\,dx}{x+b+ib}$$

Separating by means of partial fractions, integration

is now possible. Integration will give an expression of the form: $i.\ln(\alpha+\beta)$, and noting that $i.\ln(\alpha+\beta) = i.\ln|\alpha+\beta| - \tan^{-1}\left(\frac{\beta}{\alpha}\right)$, the real part, $\tan^{-1}\left(\frac{\beta}{\alpha}\right)$ is taken. The integral (real part) becomes:

$$\text{Integral} = -2\tan^{-1}\left[\frac{b}{x+b}\right] + \frac{\pi}{2}$$

and substituting into (A-11) gives:

$$\tan^{-1}\left[\frac{C_1\omega R}{V_2+C_1\omega R}\right] - \frac{\pi}{4} = \frac{z}{2C_1^2R} \qquad \text{(A-14)}$$

Rearranging (A-14) gives:

$$V_z = C_1\omega R\left(\cot\left[\frac{z}{2C_1^2R} + \frac{\pi}{4}\right] - 1\right) \qquad \text{(A-15)}$$

Since $V_z < C_1\omega R$, equation (A-9) can be written as:

$$V_R \simeq V_z + C_1\omega R \qquad \text{(A-16)}$$

and substituting (A-15) into (A-16) gives:

$$V_R = C_1\omega R \cot\left[\frac{z}{2C_1^2R} + \frac{\pi}{4}\right] \qquad \text{(A-17)}$$

Equation (A-17) gives the velocity profile for the radial component as a function of the vertical distance z, where z is positive. When z = 0, i.e. at the centreline, the radial velocity is:

$$V_R = C_1\omega R \quad (z = 0)$$

where $C_1 = 0.614$ for $k = 1/2$

and $C_1 = 0.707$ for $k = 0$

Integrating (A-17) between 0 and W/2, and multiplying by 2 and by $2\pi R$ gives the pumping capacity, as shown in the following equation:

$$Q = 2\pi^2 D^3 N C_1^3 \ln\left[\frac{\sin\left(\frac{W}{2C_1^2 D} + \frac{\pi}{4}\right)}{\sin\frac{\pi}{4}}\right]. \qquad \text{(A-18)}$$

Equation (A-18) can be simplified to the form:

$$Q = K_{t_2} N D^3 \qquad \text{where } K_{t_2} = f\,(W/D,\ k)$$

For W/D = 1/5, as is the case in most of this work, the pumping capacity expression is evaluated and:

$$K_{t_2} = 0.946 \quad \text{for } k = 1/2$$

$$K_{t_2} = 1.17 \quad \text{for } k = 0$$

The angle of flow, θ can be found from:

$$\tan\theta = \frac{\omega R}{V_R}$$

Substituting (A-17) for V_R, the following expression is obtained:

$$\tan\theta = \frac{1}{C_1} \cdot \tan\left[\frac{z}{2C_1^2 R} + \frac{\pi}{4}\right] \qquad \text{(A-19)}$$

APPENDIX III

Direction of Flow with Increasing Radial Distance

It is desired to show that the direction of flow in the turbine jet becomes more radial as the radial distance increases. Part of this effect results from the decreased tangential velocity near the tank walls because of the presence of baffles. However, an important effect is due to the geometry of the system. Figure 32 demonstrates this clearly:

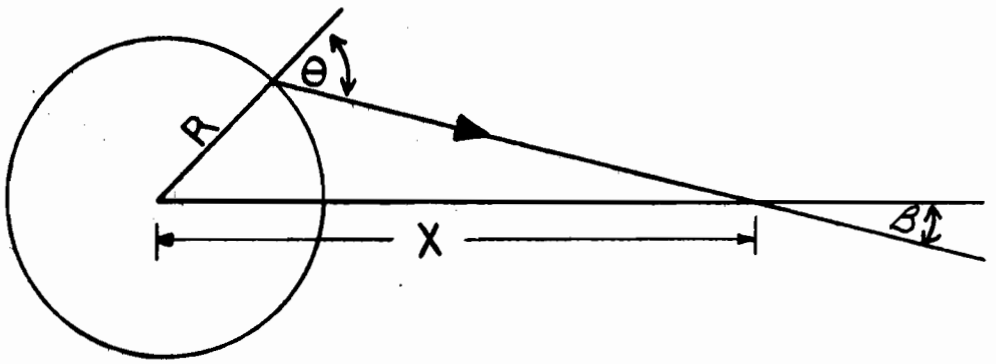

FIGURE 32. Relationship between β and θ

If θ is the angle of flow at the turbine periphery, and β the angle of flow at some radial distance X, it is evident that $\beta < \theta$ and in fact, it can be shown that:

$$\sin\beta = \frac{R}{X} \cdot \sin\theta \qquad \text{(A-20)}$$

As the radial distance X increases, β decreases and the flow becomes more radial in direction.

APPENDIX IV

Relationship between Intensity of Segregation and Pumping Capacity

Suppose two different streams are entering a continuous flow stirred tank of volume V. The first stream containing component A of concentration a has a flow rate of v_a; the other stream containing no A, has flow rate v_o, and the total flow in is F.

The fraction of particles in the tank having age between t and t+dt for a system of ideal residence time distribution is:

$$I \text{ (age distribution)} = e^{-t/\theta} \cdot dt \qquad \text{(A-21)}$$

where $\theta = V/F$

Within the tank there is an internal loop or recirculation having a flow rate Q. Of the particles having age between t and t+dt, a certain fraction will have passed through the impeller, which is given by the following distribution:

$$E(t) = \frac{1}{\theta'} \cdot e^{-t/\theta'} \qquad \text{(A-22)}$$

where $\theta' = V/Q$

So the fraction of particles in the tank having age between t and t+dt and having passed through the impeller is:

$$\text{fraction} = e^{-t/\theta} \cdot \frac{1}{\theta'} \cdot e^{-t/\theta'} \cdot dt \qquad \text{(A-23)}$$

If the entire contents of the tank are considered, particles have

ages ranging from zero to infinity. The fraction of particles in the tank having passed through the impeller is then the sum of the fractions at different ages that have passed through the impeller, and is given by:

$$\text{fraction through impeller} = \int_0^\infty \frac{1}{\theta'} e^{-t/\theta'} \, dt$$

$$= \frac{1}{\frac{\theta'}{\theta} + 1}$$

$$= \frac{Q}{Q + F} \qquad \text{(A-24)}$$

The fraction of particles in the tank that have not passed through the impeller is then $1 - Q/(Q + F) = F/(Q + F)$, and since the outlet stream is representative of the contents of the tank, the unmixed fraction in the exit stream is $F/(Q + F)$. Having obtained the unmixed fraction in the outlet stream, the intensity of segregation can be found, by considering the concentration fluctuations resulting from mixed and unmixed clumps or particles in the exit stream.

If the concentration in the outlet stream is measured for a long period of time, and molecular diffusion is neglected, the following concentrations will be noted:

(i) most clumps will have an average concentration = $\bar{a}$.

This is the fraction of material in the exit stream that is perfectly mixed, representing $Q/(Q + F)$ of the total exit stream, and having concentration $\bar{a} = a.v_a/F$.

(ii) some material will consist of clumps of pure A, having concentration a, and representing a fraction $v_a/(Q + F)$ of the total stream.

(iii) some material contains no A (zero concentration), and this represents fraction $v_o/(Q + F)$ of the total stream. Note that $(Vo + Va) = F$.

Grouping clumps of like concentration together, the situation can be described schematically in Figure 33 below:

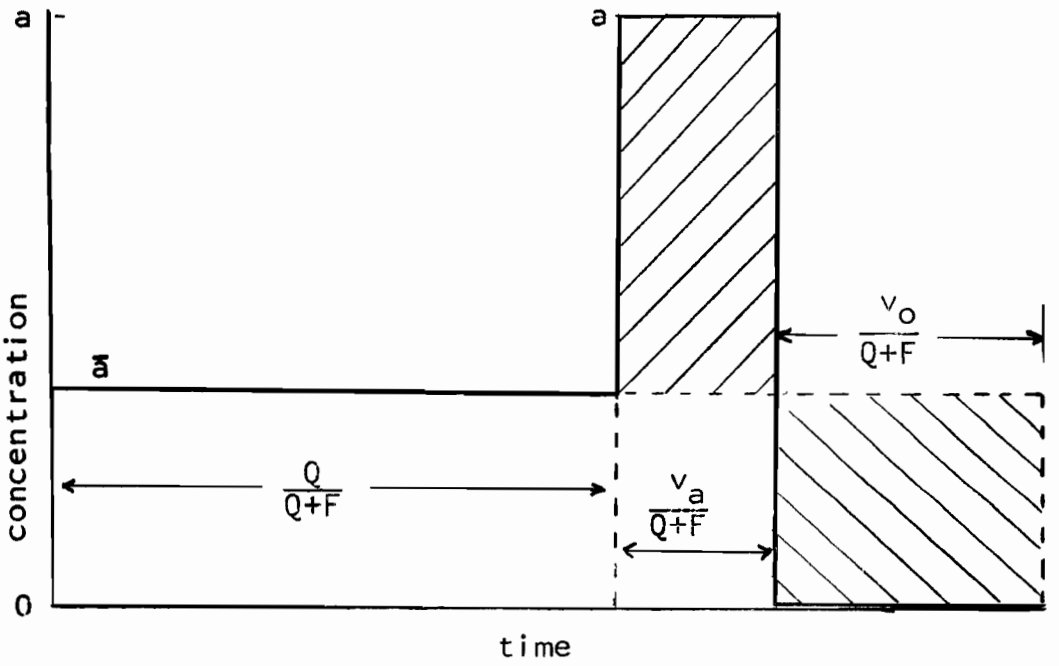

FIGURE 33. Outlet concentration fluctuations

Then σ_a^2 is represented by the sum of the squares of the cross-hatched areas:

$$\sigma_a^2 = \frac{1}{T}\int_0^{\infty} (a - \bar{a})^2 dT \qquad T \to \infty$$

$$= \frac{v_a}{Q+F}\left(a - \frac{v_a . a}{F}\right)^2 + \frac{v_o}{Q+F}\left(\frac{v_a . a}{F}\right)^2$$

$$\sigma_a^2 = \frac{v_a . a^2}{Q+F}\left(1 - \frac{v_a}{F}\right) \qquad \text{(A-25)}$$

Substituting σ_a^2 into Danckwerts' equation for intensity of segregation yields:

$$I = \frac{\sigma_a^2}{a(1-a)}$$

$$I = \frac{v_a . a^2 \left(1 - \frac{v_a}{F}\right)\frac{1}{Q+F}}{\frac{v_a . a}{F} \cdot \frac{v_o . a}{F}}$$

and finally $I = \frac{F}{Q+F}$ (A-26)

APPENDIX V. TABLES OF RESULTS

1. RESULTANT VELOCITY AND ANGLE OF FLOW IN DISCHARGE JET AT TURBINE PERIPHERY

3" Turbine in Water (D:W:L = 20:4:5)

Vertical distance z, in.	200 R.P.M.		300 R.P.M.		400 R.P.M.		500 R.P.M.		600 R.P.M.	
	V in/sec	θ°	V in/sec	θ°	V in/sec	θ°	V in/sec	θ°	V in/sec	θ°
0.30	7.7	61	14.4	67	9.5	65	5.5	60	18.1	66
0.25	15.4	66	22.5	68	25.6	72	21.2	58	34.5	71
0.20	20.4	64	27.3	66	35.4	70	37.4	62	46.7	69
0.15	25.0	62	38.6	63	44.4	66	52.1	58	62.3	62
0.10	31.8	56	46.0	58	50.6	60	63.9	54	74.0	56
0.05	34.5	52	50.0	52	54.6	54	70.1	50	80.8	50
0	34.4	51	50.9	50	55.2	51	71.4	49	82.1	48
-0.05	34.5	51	50.3	52	54.1	55	69.3	51	80.3	50
-0.10	31.8	57	46.0	56	50.6	60	62.3	52	73.3	55
-0.15	28.9	60	38.6	61	45.7	65	51.8	57	60.6	61
-0.20	23.2	64	29.9	64	36.2	69	38.6	60	47.0	67
-0.25	18.1	66	24.4	68	26.2	72	22.5	58	34.1	69
-0.30	12.2	66	16.4	68	18.9	66	5.5	60	20.4	72
Q ft^3/min	2.81		3.74		3.81		5.40		5.99	
K_{t_2}	0.892		0.798		0.610		0.692		0.638	

TABLES OF RESULTS (cont.)

2. RESULTANT VELOCITY AND ANGLE OF FLOW IN DISCHARGE JET AT TURBINE PERIPHERY

4" Turbine in Water (D:W:L = 20:4:5)

Vertical distance, z, in.	100 R.P.M.		150 R.P.M.		200 R.P.M.		250 R.P.M.		300 R.P.M.	
	V in/sec	θ°	V in/sec	θ°	V in/sec	θ°	V in/sec	θ°	V in/sec	θ°
0.4	3.9	67	9.5	62	9.5	62	18.9	66	21.2	62
0.3	10.2	61	16.4	67	20.8	66	32.3	67	33.7	66
0.2	14.4	61	23.8	65	33.2	65	46.7	63	49.1	65
0.1	21.2	58	31.4	58	45.7	56	56.0	56	61.1	58
0	23.2	51	34.1	52	48.8	51	57.5	52	66.2	53
-0.1	21.5	55	31.4	54	47.0	55	53.5	60	63.2	58
-0.2	16.4	61	25.6	62	37.4	63	45.4	66	50.9	66
-0.3	9.5	64	18.1	66	20.4	68	28.9	69	34.5	68
-0.4	3.9	68	9.5	64	10.9	68	19.7	69	20.4	68
Q ft^3/min	2.78		4.20		5.73		7.15		7.97	
K_{t_2}	0.750		0.756		0.774		0.772		0.714	

TABLES OF RESULTS (cont.)

3. RESULTANT VELOCITY AND ANGLE OF FLOW IN DISCHARGE JET AT TURBINE PERIPHERY

5" Turbine in Water (D:W:L = 20:4:5)

Vertical distance z, in.	100 R.P.M.		150 R.P.M.		200 R.P.M.		250 R.P.M.		275 R.P.M.	
	V in/sec	θ°	V in/sec	θ°	V in/sec	θ°	V in/sec	θ°	V in/sec	θ°
0.5	7.7	62	12.2	62	15.4	58	21.8	57	22.5	59
0.4	10.9	69	17.3	63	22.5	60	31.4	60	34.5	60
0.3	17.3	63	27.3	63	37.8	61	47.0	61	50.9	61
0.2	22.5	59	35.8	59	47.0	58	62.0	57	66.7	59
0.1	26.8	53	41.9	52	55.4	51	70.6	52	77.4	52
0	28.9	49	44.4	48	58.1	47	74.1	48	81.2	48
-0.1	27.3	53	42.7	51	55.4	50	71.0	52	78.8	52
-0.2	23.8	60	37.0	58	47.9	58	62.0	57	67.8	57
-0.3	18.1	62	28.4	63	35.8	60	47.3	61	50.6	62
-0.4	13.4	68	18.9	63	23.2	64	28.9	65	32.8	63
-0.5	7.7	62	10.9	62	13.4	58	16.4	55	19.7	59
Q ft^3/min	5.67		9.14		12.31		15.74		17.08	
K_{t_2}	0.784		0.842		0.850		0.870		0.859	

TABLES OF RESULTS (cont.)

4. RESULTANT VELOCITY AND ANGLE FLOW IN DISCHARGE JET AT TURBINE PERIPHERY

6" Turbine in Water (D:W:L = 20:4:5)

Vertical distance z, in.	50 R.P.M.		100 R.P.M.		125 R.P.M.		150 R.P.M.		170 R.P.M.	
	V in/sec	θ^o	V in/sec	θ^o	V in/sec	θ^o	V in/sec	θ^o	V in/sec	θ^o
0.6	7.7	62	10.9	62	13.4	55	14.4	64	17.3	62
0.5	10.9	60	14.4	60	18.1	59	19.7	59	23.8	58
0.4	14.4	58	19.7	59	24.4	60	27.8	61	33.2	60
0.3	18.9	58	25.0	59	31.4	59	39.0	61	44.4	58
0.2	21.8	56	29.9	55	38.2	56	45.7	55	53.2	54
0.1	23.8	50	33.2	50	41.6	50	51.2	51	58.1	49
0	25.6	48	34.5	48	43.0	48	53.8	48	59.8	47
-0.1	24.4	50	34.1	50	41.9	50	52.7	50	58.6	49
-0.2	21.8	56	31.4	55	39.4	54	47.6	54	52.9	54
-0.3	18.1	58	25.6	59	32.8	59	40.5	58	44.7	57
-0.4	15.4	58	21.2	61	26.2	61	29.9	62	34.5	60
-0.5	10.9	58	15.4	62	18.9	61	21.1	63	23.8	60
-0.6	7.7	58	10.9	63	14.4	57	15.4	56	17.3	56
Q ft^3/min	8.06		10.96		13.82		16.62		19.30	
K_{t_2}	1.29		0.879		0.884		0.886		0.908	

TABLES OF RESULTS (cont.)

5. RESULTANT VELOCITY AND ANGLE OF FLOW IN DISCHARGE JET AT TURBINE PERIPHERY

4" Turbine in Air (D:W:L = 20:4:5)

Vertical distance z, in.	200 R.P.M.		300 R.P.M.		366 R.P.M.		500 R.P.M.		600 R.P.M.	
	V in/sec	θ°	V in/sec	θ°	V in/sec	θ°	V in/sec	θ°	V in/sec	θ°
0.4	13.1	68	21.3	68	22.8	68	28.4	68	35.0	68
0.3	15.6	66	22.8	66	30.9	66	37.9	66	46.0	66
0.2	22.3	65	35.0	65	43.4	65	56.3	65	70.7	65
0.1	35.0	58	51.4	58	73.1	58	91.9	58	109.1	58
0	43.4	53	60.5	53	86.2	53	121.2	53	144.2	53
-0.1	37.9	58	53.3	58	75.6	58	104.2	58	130.4	58
-0.2	24.9	66	35.0	66	48.6	66	64.9	66	86.2	66
-0.3	16.4	68	22.8	68	30.9	68	40.2	68	53.3	68
-0.4	12.4	68	19.0	68	22.8	68	29.6	68	35.7	68
Q ft^3/min	4.43		6.38		8.79		11.71		14.42	
K_{t_2}	0.598		0.574		0.648		0.632		0.650	

TABLES OF RESULTS (cont.)

6. RESULTANT VELOCITY AND ANGLE OF FLOW IN DISCHARGE JET AT TURBINE PERIPHERY

5" Turbine in Air (D:W:L = 20:4:5)

Vertical distance z, in.	200 R.P.M.		300 R.P.M.		400 R.P.M.		500 R.P.M.		600 R.P.M.	
	V in/sec	θ^o	V in/sec	θ^o	V in/sec	θ^o	V in/sec	θ^o	V in/sec	θ^o
0.5	14.8	59	21.6	59	27.8	59	35.3	59	43.3	59
0.4	18.6	60	26.0	60	35.3	60	46.0	60	54.7	60
0.3	23.7	61	35.3	61	46.0	61	61.2	61	73.2	61
0.2	33.8	59	50.7	59	71.9	59	92.9	59	112.8	59
0.1	43.3	52	68.2	52	94.5	52	123.9	52	148.4	52
0	47.8	48	73.2	48	105.9	48	133.7	48	159.6	48
-0.1	44.2	52	68.2	52	97.6	52	125.8	52	150.6	52
-0.2	35.3	57	56.8	57	75.8	57	100.9	57	118.2	57
-0.3	25.4	62	37.6	62	53.7	62	65.8	62	79.9	62
-0.4	18.6	63	26.6	63	36.0	63	47.8	63	56.8	63
-0.5	14.4	59	20.1	59	27.2	59	35.3	59	42.5	59
Q ft^3/min	9.34		14.21		19.81		25.60		30.63	
K_{t_2}	0.646		0.654		0.684		0.708		0.706	

TABLES OF RESULTS (cont.)

7. RESULTANT VELOCITY AND ANGLE OF FLOW IN DISCHARGE JET AT TURBINE PERIPHERY

6" Turbine in Air (D:W:L = 20:4:5)

Vertical distance z, in.	100 R.P.M.		200 R.P.M.		300 R.P.M.		500 R.P.M.		600 R.P.M.	
	V in/sec	θ°	V in/sec	θ°	V in/sec	θ°	V in/sec	θ°	V in/sec	θ°
0.6	11.8	62	21.5	62	28.9	62	45.9	62	53.5	62
0.5	14.5	60	25.6	60	33.0	60	53.5	60	63.1	60
0.4	16.0	59	30.0	59	39.8	59	64.1	59	77.4	59
0.3	21.3	59	38.4	59	54.4	59	90.0	59	108.5	59
0.2	25.5	55	50.0	55	71.6	55	123.0	55	140.7	55
0.1	30.9	50	61.1	50	83.5	50	148.2	50	172.8	50
0	34.3	48	65.2	48	90.0	48	160.2	48	186.2	48
-0.1	32.9	50	61.1	50	83.5	50	152.1	50	177.2	50
-0.2	27.8	55	51.7	55	71.6	55	129.8	55	150.3	55
-0.3	23.9	59	41.2	59	56.3	59	101.1	59	116.4	59
-0.4	18.1	61	31.2	61	41.2	61	68.3	61	83.5	61
-0.5	14.1	62	25.6	62	33.0	62	56.3	62	66.2	62
-0.6	11.8	63	21.3	63	28.9	63	46.7	63	53.5	63
Q $ft.^3$/min	10.09		23.21		25.70		44.79		52.36	
K_{t_2}	0.808		0.928		0.686		0.716		0.698	

TABLES OF RESULTS (cont.)

8. RESULTANT VELOCITY AND ANGLE OF FLOW IN DISCHARGE JET OF TURBINES AT DIFFERENT RADIAL DISTANCES

(4" Turbine in Water at 280 R.P.M.)

Vertical distance z, in.	R* = 2"		R = 2.5"		R = 3"		R = 4"		R = 5"	
	V in/sec	θ°	V in/sec	θ°	V in/sec	θ°	V in/sec	θ°	V in/sec	θ°
0.4	14.4	64	5.5	71	14.4	54	16.4	34	15.4	30
0.3	33.2	65	19.7	62	21.8	46	21.8	30	19.7	26
0.2	49.1	62	35.0	54	28.4	44	23.8	30	19.7	26
0.1	61.5	54	43.3	48	34.1	40	26.2	29	19.7	26
0	65.8	50	46.7	44	38.2	38	27.3	28	19.7	26
-0.1	60.6	56	44.7	47	35.8	38	26.8	28	19.7	26
-0.2	49.4	63	36.2	52	29.9	42	25.6	28	19.7	26
-0.3	32.8	68	21.8	60	20.4	46	22.5	28	19.7	26
-0.4	18.1	68	9.5	71	15.4	50	18.9	32	17.3	30
Q $ft.^3$/min	8.32		8.64		10.84		14.61		15.06	

*R = Radial distance from centre

TABLES OF RESULTS (cont.)

9. RESULTANT VELOCITY AND ANGLE OF FLOW IN DISCHARGE JET FOR TURBINES OF DIFFERENT BLADE WIDTHS

(4" Turbine in Water at 100 R.P.M.)

Vertical distance z, in.	W = 1.6"		W = 1.4"		W = 1.2"		W = 1.0"		W* = 0.6"	
	V in/sec	θ°	V in/sec	θ°	V in/sec	θ°	V in/sec	θ°	V in/sec	θ°
0.8	0	-								
0.7	0	-	0	-						
0.6	0	-	0	-	0	-				
0.5	0	-	0	-	0	-	0	-		
0.4	6.7	40	7.7	50	5.5	38	0	-		
0.3	16.4	40	16.4	36	12.2	38	9.5	62	10.9	72
0.2	22.5	44	19.7	42	18.9	39	16.4	56	16.4	62
0.1	23.8	45	22.5	41	23.2	40	21.2	52	20.4	54
0	24.4	45	23.2	40	23.8	39	21.8	49	21.8	50
-0.1	24.4	45	21.8	42	23.8	40	21.8	52	21.1	53
-0.2	22.5	44	19.7	42	20.4	40	17.3	56	16.4	62
-0.3	18.1	40	15.4	36	12.2	38	10.9	62	10.9	72
-0.4	6.7	40	5.5	50	5.5	38	0	-		
-0.5	0	-	0	-	0	-	0	-		
-0.6	0	-	0	-	0	-				
-0.7	0	-	0	-						
-0.8	0	-								
Q ft^3/min	5.38		5.22		4.99		3.09		2.57	

*W = 0.8" given in Table 2

TABLES OF RESULTS (cont.)

10. RESULTANT VELOCITY AND ANGLE OF FLOW IN DISCHARGE JET FOR TURBINES OF DIFFERENT BLADE WIDTHS

(4" Turbine in Water at 200 R.P.M.)

Vertical distance z, in.	W = 1.6"		W = 1.4"		W = 1.2"		W = 1.0"		W* = 0.6"	
	V in/sec	θ°	V in/sec	θ°	V in/sec	θ°	V in/sec	θ°	V in/sec	θ°
0.8	0	-								
0.7	0	-	0	-						
0.6	0	-	0	-	0	-				
0.5	0	-	0	-	0	-	5.5	72		
0.4	23.8	34	12.2	32	10.9	45	12.2	64		
0.3	33.2	40	30.9	36	27.3	40	23.2	56	18.1	70
0.2	40.9	44	42.3	39	41.2	40	35.8	56	27.8	64
0.1	42.7	44	45.4	40	46.0	41	43.0	51	38.6	56
0	44.4	44	45.4	40	46.7	38	45.7	46	40.9	51
-0.1	43.0	44	45.4	40	46.3	40	44.4	51	39.4	56
-0.2	40.9	44	43.0	39	41.2	41	36.6	56	29.4	64
-0.3	36.2	40	30.9	36	27.8	40	23.2	56	18.1	70
-0.4	17.3	34	10.9	30	10.9	44	13.4	63		
-0.5	0	-	0	-	0	-	5.5	72		
-0.6	0	-	0	-	0	-				
-0.7	0	-	0	-						
-0.8	0	-								
Q ft^3/min	10.56		10.61		10.00		7.25		4.44	

*W = 0.8" given in Table 2

TABLES OF RESULTS (cont.)

II. AXIAL VELOCITIES AND YAW* ANGLES

(8" Propeller in Water)

Radial Distance from Centre r inches	200 R.P.M.		250 R.P.M.		Radial Distance from Centre r inches	300 R.P.M.	
	V_{axial} in/sec	Yaw ^{o}	V_{axial} in/sec	Yaw ^{o}		V_{axial} in/sec	Yaw ^{o}
4.0	9.1	47	12.2	42	4.0	12.5	46
3.8	11.8	44	13.6	42	3.9	13.9	45
3.6	13.9	40	15.3	42	3.7	15.2	42
3.4	17.0	34	19.5	36	3.5	19.2	38
3.2	18.9	33	20.8	34	3.3	23.6	34
3.0	21.4	29	25.0	30	3.1	29.7	28
2.8	22.4	29	26.2	29	2.9	30.9	28
2.6	23.4	29	27.8	29	2.7	32.0	30
2.4	24.4	29	29.1	29	2.5	35.1	28
2.2	24.8	29	28.5	28	2.3	34.5	28
2.0	24.8	29	28.2	28	2.1	34.4	27
1.5	21.9	29	26.9	28	1.9	34.0	27
1.0	23.5	30	24.5	30	1.7	33.8	28
0.5	20.1	30	19.9	32	1.5	33.4	28
0	0	-	0	-	1.0	24.1	30
					0.5	20.7	32
					0	0	-
Q ft^3/min	34.26		39.40			46.14	
K_p	0.58		0.53			0.52	

*where yaw angle is the inclination from the vertical in the plane perpendicular to the radius

TABLES OF RESULTS (cont.)

12. AXIAL VELOCITY AND YAW* ANGLES

(8" Propeller in Air)

Radial Distance from Centre r inches	200 R.P.M.		300 R.P.M.	
	V_{axial} in/sec	Yaw ^{o}	V_{axial} in/sec	Yaw ^{o}
4.0	16.7	47	16.7	46
3.8	18.9	44	24.1	45
3.6	18.9	40	25.2	42
3.4	18.9	34	26.4	38
3.2	18.9	33	27.0	34
3.0	21.4	29	30.2	28
2.8	21.4	29	30 9	28
2.6	21.4	29	30.9	30
2.4	21.4	29	31.5	28
2.2	18.9	29	28.9	28
2.0	16.7	29	27.0	27
1.5	14.7	29	23.0	28
1.0	12.8	30	18.9	28
0.5	10.2	30	24.1	32
0	0	-	0	-
Q ft^3/min	31.82		45.65	
K_p	0.54		0.51	

*where yaw angle is the inclination from the vertical in the plane perpendicular to the radius

TABLES OF RESULTS (cont.)

13. MATERIAL BALANCE

(4" Turbine in Water at 300 R.P.M.)

Horizontal Traverse			Vertical Traverse		
Radial Distance from Centre r inches	V_{axial} in/sec	Pitch* Angle o	Vertical Distance z, in	$V_{resultant}$ in/sec	θ o
2.0	10.9	0	0.4	21.1	62
1.8	12.2	0	0.3	33.7	66
1.6	12.2	0	0.2	49.1	65
1.4	12.7	20	0.1	61.1	58
1.2	12.1	28	0	66.2	53
1.0	9.0	37	-0.1	63.2	58
0.8	8.1	33	-0.2	50.9	66
0.6	9.0	18	-0.3	34.5	68
0.4	9.0	18	-0.4	20.4	68
0.2	9.0	18			
0	0	-			
Q $ft.^3$/min	8.50			7.97	

*Pitch angle is the inclination from the vertical in the (r,z) plane. The yaw angle was found to be negligible.

TABLES OF RESULTS (cont.)

14. MATERIAL BALANCE

(9" Turbine in Air at 420 R.P.M.)

Horizontal Traverse		Vertical Traverse		
Radial Distance from Centre r inch	V_{axial}* in/sec	Vertical Distance z in	$V_{resultant}$ in/sec	θ^{o}
4.5	38.5	0.9	62.1	62
4.3	40.8	0.8	80.1	60
4.1	40.8	0.7	91.1	58
3.9	40.8	0.6	123.7	58
3.7	40.8	0.5	153.4	58
3.5	40.0	0.4	176.0	56
3.3	40.0	0.3	198.3	54
3.1	39.3	0.2	219.9	52
2.9	36.3	0.1	228.4	48
2.7	34.2	0	231.3	47
2.5	32.8	-0.1	219.9	48
2.3	27.8	-0.2	206.2	52
2.1	26.6	-0.3	180.8	54
1.9	23.4	-0.4	157.7	56
1.7	22.3	-0.5	131.2	58
1.5	20.4	-0.6	101.7	58
1.0	16.9	-0.7	80.1	58
0.5	14.9	-0.8	73.7	60
0	14.9	-0.9	62.1	62
Q $ft.^3$/min	153.0		156.0	

*Velocity measurements were made sufficiently far from the turbine (1") that yaw and pitch angles were negligible